

This is a repository copy of *The evolutionary origins of the cat attractant nepetalactone in catnip*.

White Rose Research Online URL for this paper:
<https://eprints.whiterose.ac.uk/161043/>

Version: Published Version

Article:

Lichman, Benjamin Robert orcid.org/0000-0002-0033-1120, Godden, Grant, Hamilton, John et al. (14 more authors) (2020) The evolutionary origins of the cat attractant nepetalactone in catnip. *Science Advances*. eaba0721. ISSN 2375-2548

<https://doi.org/10.1126/sciadv.aba0721>

Reuse

This article is distributed under the terms of the Creative Commons Attribution-NonCommercial (CC BY-NC) licence. This licence allows you to remix, tweak, and build upon this work non-commercially, and any new works must also acknowledge the authors and be non-commercial. You don't have to license any derivative works on the same terms. More information and the full terms of the licence here:
<https://creativecommons.org/licenses/>

Takedown

If you consider content in White Rose Research Online to be in breach of UK law, please notify us by emailing eprints@whiterose.ac.uk including the URL of the record and the reason for the withdrawal request.

BIOSYNTHESIS

The evolutionary origins of the cat attractant nepetalactone in catnip

Benjamin R. Lichman^{1*}, Grant T. Godden², John P. Hamilton³, Lira Palmer⁴, Mohamed O. Kamileen⁴, Dongyan Zhao^{3†}, Brienne Vaillancourt³, Joshua C. Wood³, Miao Sun², Taliesin J. Kinser^{2,5}, Laura K. Henry⁶, Carlos Rodriguez-Lopez⁴, Natalia Dudareva^{6,7,8}, Douglas E. Soltis^{2,5}, Pamela S. Soltis², C. Robin Buell^{3,9,10*}, Sarah E. O'Connor^{4*}

Catnip or catmint (*Nepeta* spp.) is a flowering plant in the mint family (Lamiaceae) famed for its ability to attract cats. This phenomenon is caused by the compound nepetalactone, a volatile iridoid that also repels insects. Iridoids are present in many Lamiaceae species but were lost in the ancestor of the Nepetoideae, the subfamily containing *Nepeta*. Using comparative genomics, ancestral sequence reconstructions, and phylogenetic analyses, we probed the re-emergence of iridoid biosynthesis in *Nepeta*. The results of these investigations revealed mechanisms for the loss and subsequent re-evolution of iridoid biosynthesis in the *Nepeta* lineage. We present evidence for a chronology of events that led to the formation of nepetalactone biosynthesis and its metabolic gene cluster. This study provides insights into the interplay between enzyme and genome evolution in the origins, loss, and re-emergence of plant chemical diversity.

INTRODUCTION

Plants from the genus *Nepeta* L. are commonly known as catmint or catnip due to their ability to modify the behavior of cats. Catnip affects approximately two-thirds of domestic cats and many wild felid species including lions, tigers, and ocelots (1) and induces playful actions such as rolling over, cheek rubbing, and pawing (2). The responsible agents are nepetalactones, volatile metabolites thought to mimic cat pheromones (Fig. 1A). Most likely, the adaptive function of nepetalactones in *Nepeta* is to protect against herbivorous insects (3), not to stimulate cats; notably, nepetalactones can repel insects with efficiencies comparable to the synthetic repellent *N,N*-diethyl-*meta*-toluamide (DEET) (4). Furthermore, *Nepeta* species produce different nepetalactone stereoisomers, with their ratio affecting the effectiveness of insect repellence (4).

Nepetalactones are iridoids, a class of atypical monoterpenes that act as defensive compounds in some flowering plants. Iridoid biosynthesis begins with hydrolysis of geranyl pyrophosphate, catalyzed by geraniol synthase (GES), followed by oxidation, catalyzed by geraniol 8-hydroxylase (G8H) and 8-hydroxygeraniol oxidoreductase (HGO), yielding the precursor 8-oxogeraniol (8OG) (Fig. 1B) (5). The first committed step into the iridoid pathway is the reductive cyclization of 8OG into nepetalactol, catalyzed by iridoid synthase (ISY) (6).

We initiated elucidation of the biosynthetic basis of the three major nepetalactone stereoisomers found in *Nepeta* species and determined

that *Nepeta* ISYs are not responsible for determining nepetalactone stereochemistry (7). Instead, ISYs catalyze the reduction of 8OG but do not control the subsequent cyclization. These enzymes yield a reactive intermediate that, without partner enzymes present, spontaneously cyclizes to form a mixture of products including *cis-trans*-nepetalactol (8, 9).

In *Nepeta mussinii*, several enzymes act in combination with ISY to control the formation of nepetalactone stereoisomers (Fig. 1C) (9). Three nepetalactol-related short-chain reductase/dehydrogenases (NEPS1, NEPS2, and NEPS3) were identified. NEPS1 is a dehydrogenase, catalyzing the formation of *cis-trans*-nepetalactone or *cis-cis*-nepetalactone from the corresponding nepetalactol isomer. In contrast, NEPS2 and NEPS3 appear to act as cyclases: NEPS2 was found to promote the formation of *cis-trans*-nepetalactol, while NEPS3 promotes the formation of *cis-cis*-nepetalactol, an isomer only present in trace quantities in the uncatalyzed cyclization. The enzymes responsible for the formation of the *trans-cis*-nepetalactone isomers have not been identified, yet other NEPS homologs are hypothesized to play this role.

Iridoids are widespread in the asterid subgroup of flowering plants including the mint family (Lamiaceae) to which *Nepeta* belongs (Fig. 2A) (10). Ancestral state reconstructions indicate that iridoid biosynthesis was present in the most recent common ancestor of Lamiaceae (Fig. 2) (11). Most iridoid producers in Lamiaceae produce iridoid glycosides that act as a defense against chewing insects [e.g., harpagide; Fig. 1A] (10, 12). However, the ability to produce iridoids appears to have been lost in the ancestor of the Nepetoideae lineage (a large subclade of mints), and mono- and sesquiterpene volatiles usurped them as key defensive compounds (10). However, iridoid biosynthesis re-emerged in one genus of Nepetoideae—*Nepeta*, primarily in the form of the volatile nepetalactones (Fig. 2) (10). *Nepeta* therefore has emerged as an important model to investigate the loss and subsequent evolutionary re-emergence of a major class of defensive compounds.

To uncover how *Nepeta* forms nepetalactones and how it re-evolved the ability to produce iridoids, we sequenced the genomes of two iridoid-producing species [*Nepeta cataria* L. and *Nepeta mussinii*

¹Centre for Novel Agricultural Products, Department of Biology, University of York, York YO10 5DD, UK. ²Florida Museum of Natural History, University of Florida, Gainesville, FL 32611, USA. ³Department of Plant Biology, Michigan State University, 612 Wilson Road, East Lansing, MI 48824, USA. ⁴Department of Natural Product Biosynthesis, Max Planck Institute for Chemical Ecology, D-07745 Jena, Germany. ⁵Department of Biology, University of Florida, Gainesville, FL 32611, USA. ⁶Department of Biochemistry, Purdue University, West Lafayette, IN 47907, USA. ⁷Department of Horticulture and Landscape Architecture, Purdue University, West Lafayette, IN 47907, USA. ⁸Purdue Center for Plant Biology, Purdue University, West Lafayette, IN 47907, USA. ⁹Plant Resilience Institute, Michigan State University, 612 Wilson Road, East Lansing, MI 48824, USA. ¹⁰MSU AgBioResearch, Michigan State University, 446 West Circle Drive, East Lansing, MI 48824, USA.

*Corresponding author. Email: benjamin.lichman@york.ac.uk (B.R.L.); buell@msu.edu (C.R.B.); oconnor@ice.mpg.de (S.E.O.)

†Present address: Institute of Biotechnology, Cornell University, 525 Tower Rd. Ithaca, NY 14853, USA.

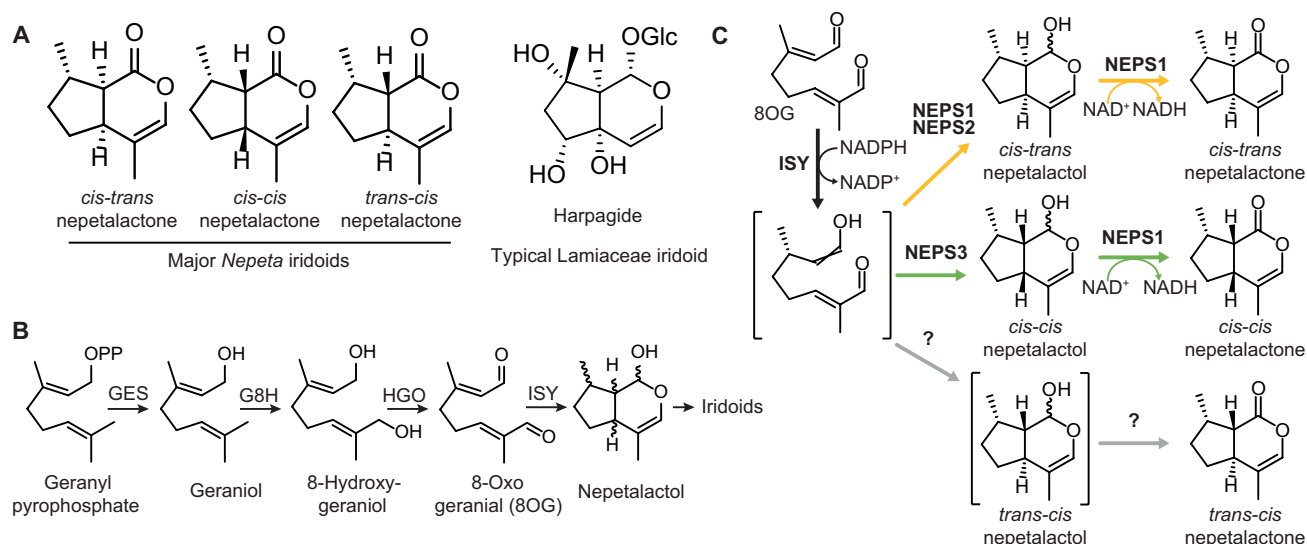


Fig. 1. Iridoid and nepetalactone biosynthesis. (A) Volatile nepetalactone stereoisomers found in *Nepeta*. Harpagide is a typical nonvolatile iridoid glucoside found in other iridoid-producing Lamiaceae. (B) Early iridoid biosynthetic pathway in plants: geraniol synthase (GES), geraniol 8-hydroxylase (G8H), 8-hydroxygeraniol oxidoreductase (HGO), and iridoid synthase (ISY). (C) Knowledge of nepetalactone biosynthesis in *N. mussinii* as reported in Lichman *et al.* (9). The crossed double bond depiction in the ISY product refers to unknown or undefined stereochemistry.

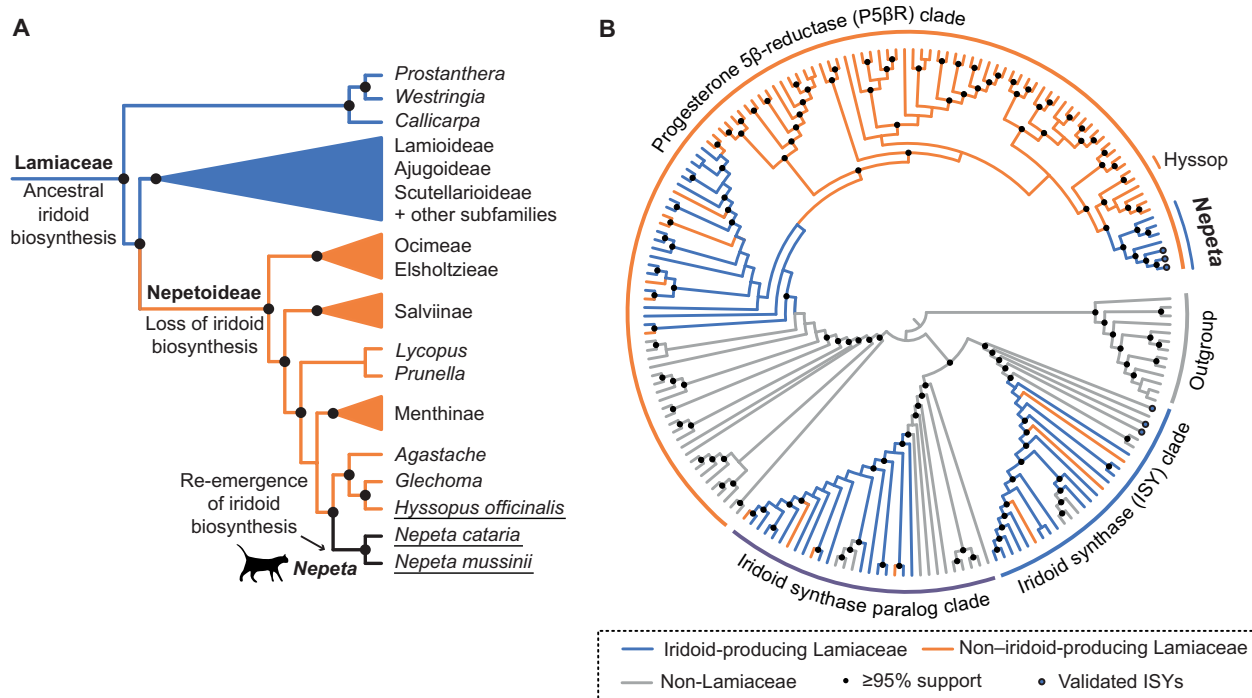


Fig. 2. Lamiaceae and ISY. (A) Phylogenetic tree of Lamiaceae species as reported in (10); black circles, bootstrap support $\geq 99\%$. (B) Cladogram of the *PRISE* gene family. See fig. S15 for annotated phylogram.

Spreng. ex. Henckel (syn. *Nepeta racemosa* Lam.) along with the closely related, non-iridoid-producing hyssop (*Hyssopus officinalis* L.). This comparative genomic approach, combined with phylogenetic analysis and enzymology of reconstructed ancestral biosynthetic enzymes, provides experimental evidence for a sequence of molecular and genomic events that led to the re-emergence of iridoids and the evolution of novel chemistry.

RESULTS

The early iridoid pathway in *Nepeta* and hyssop

The metabolite profiles of *N. cataria*, *N. mussinii*, and *H. officinalis* were analyzed to determine iridoid content (figs. S1 to S7). The major volatile components of *Nepeta* leaves and flowers are nepetalactones, which are absent from hyssop tissues. We also tentatively identified soluble iridoid glycosides (e.g., 1,5,9-epi-deoxyloganic acid) in *Nepeta*

tissues, but there was no evidence of iridoid glycosides in hyssop tissues.

Next, genome assemblies of the three species (*N. cataria*, *N. mussinii*, and *H. officinalis*) were generated (tables S1 to S4). The presence of highly conserved gene copies in *N. cataria* indicated the presence of multiple duplicated genes, consistent with a tetraploid genome, in contrast with hyssop and *N. mussinii* which are diploids (table S3). Gene candidates (*GES*, *G8H*, and *HGO*; Fig. 1C) encoding biosynthetic enzymes that yield the iridoid precursor 8OG were identified by similarity to the previously characterized sequences from the nonmint *Catharanthus roseus* (L.) G. Don of Apocynaceae, producer of the iridoid-derived anticancer compound vinblastine (figs. S8 to S10 and table S5) (5), and through tissue-specific coexpression patterns (figs. S11 to S13). The encoded enzyme candidates were recombinantly produced and analyzed for activity in vitro (fig. S14). Candidate enzymes from both *Nepeta* species demonstrated expected activities. We were also able to detect activity for the G8H candidate from hyssop, while *GES* and *HGO* candidates could not be heterologously produced with sufficient quantity or purity for biochemical assay. Thus, their activities remain uncharacterized. Notably, *GES*, *G8H*, and *HGO* genes in hyssop were lowly expressed in all tissues, which may account for the absence of iridoids in hyssop (fig. S13).

Geraniol is detected in the roots of hyssop (fig. S3). However, in hyssop, the *GES* candidate gene is not expressed in roots and its transcripts are only present in flowers, albeit at very low levels (fig. S13). The origin of this geraniol is therefore unclear. It may arise from a pathway that does not require *GES*, such as the Nudix pathway found in rose flowers (13).

ISY, which acts after *HGO* (Fig. 1C), catalyzes the first committed step in all known plant iridoid pathways (6, 7). *ISY* belongs to the PRISE (progesterone 5 β -reductase/*ISY*) enzyme family (14). Hyssop does not contain a copy of *ISY*; no Nepetoideae transcriptomes or genomes contain genes that phylogenetically group with previously characterized *ISY*s (Fig. 2B and fig. S15). In contrast, all iridoid-producing Lamiaceae species outside of Nepetoideae have a putative *ISY* gene in this clade. This suggests that the loss of iridoid biosynthesis in the entire Nepetoideae is due, in part, to the loss of the *ISY* gene. Although *ISY* genes were identified in *Nepeta*, they are not orthologous with other previously characterized *ISY*s but instead are present in a separate clade of putative progesterone 5 β -reductase orthologs (*P5 β Rs*; Fig. 2B). This finding strongly suggests that *Nepeta* regained iridoid biosynthesis through the parallel evolution of a novel *ISY* enzyme.

Identification of nepetalactone gene clusters in *Nepeta*

Having identified the major components of the iridoid pathway in *Nepeta* and hyssop, we used our three genome assemblies to analyze the genomic organization of these genes. Within the *Nepeta* genomes, iridoid biosynthetic enzymes are organized in syntenic gene clusters containing *ISY*, *NEPS* homologs, and major latex protein-like genes (*MLPL*) (Fig. 3A). Clusters of functionally related nonhomologous genes are a feature of a subset of plant metabolic pathways, although the exact role of these genomic clusters is currently unclear (15). Two gene clusters were identified in *N. cataria* and one in *N. mussinii*. As *N. cataria* is a tetraploid and *N. mussinii* a diploid, this distribution indicates that the cluster formation predated the emergence of either species. The cluster in *N. mussinii* also features *GES*, which is absent from both *N. cataria* clusters.

Although the core *ISY*, *NEPS*, and *MLPL* gene content is conserved, the gene order, orientation, and *NEPS* content differ between the three clusters. However, it is unclear whether this reduced local synteny is unique to this region or reflects a genome-wide trend. In the syntenic location in the hyssop genome, a *NEPS*-like gene is present but no *PRISE/ISY* or *GES* gene was identified. Gene expression analyses in *N. cataria* and *N. mussinii* revealed that clustered and nonclustered iridoid biosynthetic genes, including the previously unreported *MLPL* and *NEPS* homologs (*NEPS4* and *NEPS5*), are coordinately expressed across different tissues (figs. S11 and S12).

Elucidation of nepetalactone biosynthesis pathway

The enzymes encoded by the *ISY*, *NEPS*, and *MLP*-like (*MLPL*) genes were biochemically characterized. Using different combinations of *NEPS*s and *MLPL* in the presence of *ISY* and 8OG led to the formation of the three distinct nepetalactone stereoisomers, indicating that *NEPS* and *MLPL* work in combination with *ISY* to control the stereochemical mode of 8OG cyclization (Table 1; Fig. 3, B and C; and figs. S16 to S20).

The previously observed *cis-cis* cyclase activity of NmNEPS3 was also obtained here, together with the characterization of two new NEPS3 enzymes from *N. cataria* (9). As expected, both NcNEPS3A and NcNEPS3B formed *cis-cis*-nepetalactol (Table 1 and fig. S18). While NmNEPS3 and NcNEPS3B do form trace quantities of *cis-cis*-nepetalactone, NcNEPS3A produced it in greater amounts (fig. S18). This indicates that it has comparatively higher dehydrogenase activity, forming *cis-cis*-nepetalactone from *cis-cis*-nepetalactol.

The previously unreported NEPS4 appears to be the missing *trans-cis*-cyclase, and NEPS1 acts as the partner dehydrogenase. This is shown for enzymes from *N. cataria* and *N. mussinii* (fig. S19). Incubation of only NmNEPS4 or NcNEPS4 with *ISY*, but not the other NEPS, causes the formation of *trans-cis*-iridodial and *cis-trans*-nepetalactone. When NEPS1, a dehydrogenase, is added, *trans-cis*-nepetalactone formation occurs. These results indicate that NEPS4 can cyclize the reactive *ISY* product into *trans-cis*-nepetalactol. This intermediate is released from the NEPS4 active site. However, it is unstable and, in the absence of a dehydrogenase, it will decay to *trans-cis*-iridodial (16). We have previously shown that *trans-cis*-iridodial is not a substrate for NEPS1 (9). Therefore, when NEPS1 is present, it must be taking up the reactive *trans-cis*-nepetalactol before its decay and oxidizing it into the stable *trans-cis*-nepetalactone. In this extraordinary sequence of reactions, there are two unstable intermediates moving between active sites. NEPS4 also has residual dehydrogenase activity, although this activity appears to be selective for *cis-trans*-nepetalactol over *trans-cis*-nepetalactol. This suggests that NEPS4 has separate binding modes for its cyclization and dehydrogenation activities.

We previously demonstrated that NEPS1 could catalyze the dehydrogenation of *cis-trans*-nepetalactol and *cis-cis*-nepetalactol (9). Here, we validate these results with NmNEPS1 and NcNEPS1 (Table 1 and figs. S18 and S20). We also report the additional NEPS1 dehydrogenase activity on *trans-cis*-nepetalactol when tested with NEPS4 (Table 1 and fig. S19). The newly reported NEPS5s, from both *N. cataria* and *N. mussinii*, are dehydrogenases with similar behavior to NEPS1 (Table 1 and figs. S18 and S20). They appear to catalyze formation of *cis-trans*-, *cis-cis*- and *trans-cis*-nepetalactones, although the latter two only in conjunction with NEPS3 or NEPS4 cyclases, respectively.

Our previous observation of NmNEPS2 promoting the *cis-trans*-nepetalactol formation at the expense of side products was not confirmed

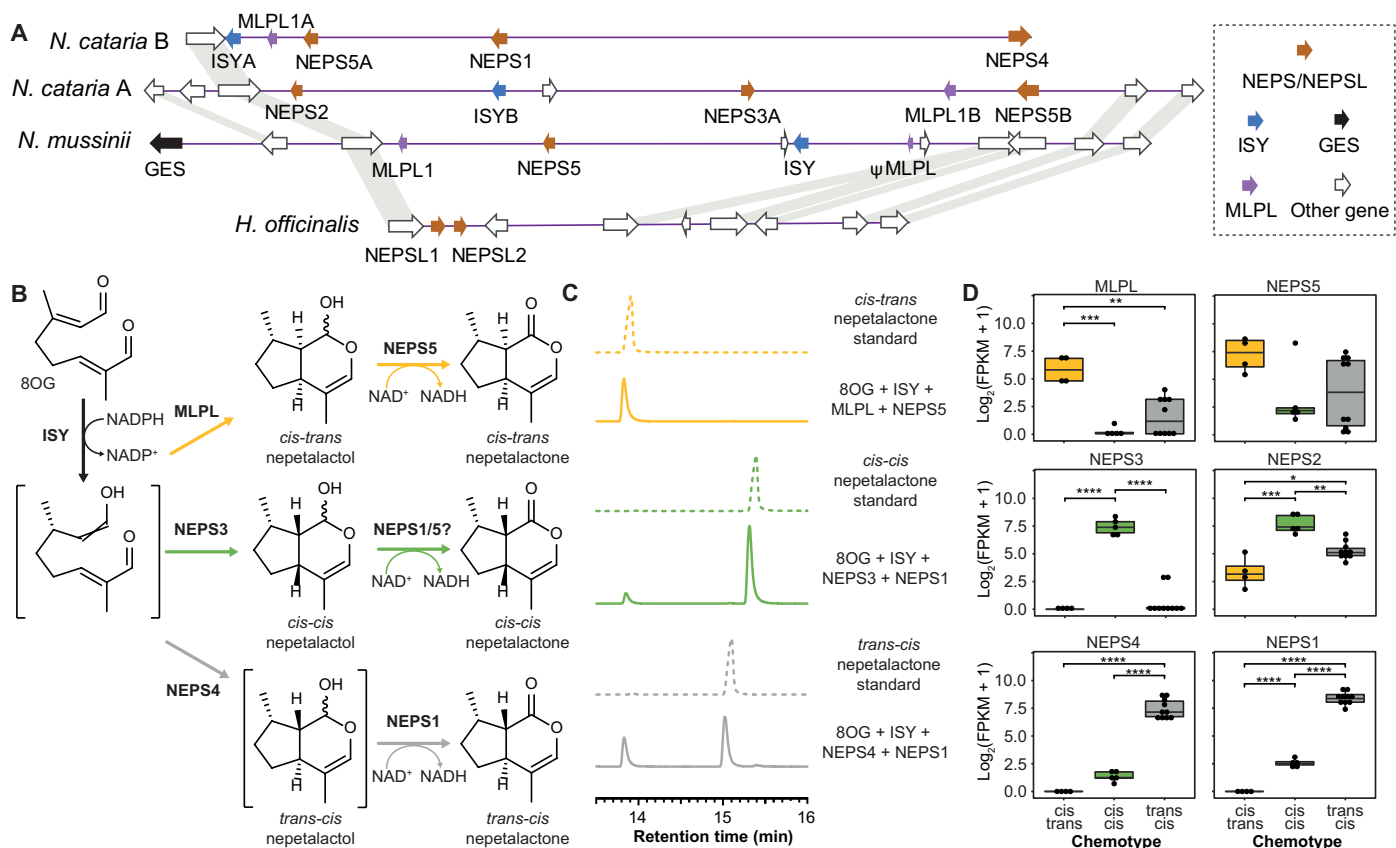


Fig. 3. Metabolic gene clusters in *Nepeta*. (A) Genomic organization and synteny relationships of nepetalactone biosynthesis gene cluster in *Nepeta*. Gray polygons show synteny relationships. (B) Biosynthetic pathway of nepetalactone stereoisomer formation based on combination of in vitro assay data and in planta gene expression. The crossed double bond depiction in the ISY product refers to unknown or undefined stereochemistry. (C) In vitro multienzyme cascade assays demonstrating selective formation of nepetalactone stereoisomers (see also figs. S16 to S20). (D) Differential expression of nepetalactone biosynthetic genes in *N. mussinii* individuals with distinct nepetalactone stereo-chemotypes. Significant differences determined by analysis of variation with Tukey's post hoc test ($n = 4$ to 10 ; **** $P < 0.0001$, *** $P < 0.001$, ** $P < 0.01$, * $P < 0.05$) (see also fig. S21).

here with NmNEPS2 and NcNEPS2. Instead, we did not detect any specific notable activity for NEPS2, either alone or in conjunction with other enzymes.

However, we have identified additional enzymes that appear to promote formation of *cis-trans*-nepetalactol when tested in conjunction with ISY. This appears to be not a NEPS but the MLPL proteins found in the gene clusters (fig. S17A). Incubation of NmMLPL with ISY caused a significant increase in *cis-trans*-nepetalactol content compared to an ISY alone or a BSA control (fig. S17C). NcMLPLA and NcMLPLB appear to have similar behaviors. Furthermore, addition of MLPL to ISY and NEPS5 reactions reduces the formation of minor *cis-cis*- and *trans-cis*-nepetalactone isomers (fig. S20B). MLPLs are part of the PR-10 family of proteins; three enzymes from this family were reported to be involved in benzyloquinoline alkaloid biosynthesis (17). They typically catalyze energetically undemanding reactions that have appreciable “spontaneous” rates in buffer or solvent. We expect that the addition of MLPL will enhance the efficiency of recombinant systems which use ISY to produce *cis-trans*-nepetalactol (18).

The NEPS and MLPL enzymes that catalyze the formation of nepetalactone isomers in *Nepeta* are found to exhibit both multiple and overlapping activities in vitro (Table 1). To determine the contribution of these enzymes to nepetalactone isomers in planta, we

compared gene expression of NEPSs and MLPL genes across accessions of *N. mussinii* with distinct nepetalactone stereo-chemotypes (Fig. 3D, fig. S21, and table S6). The expression levels of the NEPS and MLPL genes largely correlated with in planta chemistry and were concordant with in vitro activities, suggesting that NEPS and MLPL are responsible for all three nepetalactone stereoisomers observed in *N. cataria* and *N. mussinii*.

Cyclase in planta expression patterns were correlated with in vitro activities: MLPL, NEPS3, and NEPS4 expression were highest in plants primarily producing *cis-trans*-, *cis-cis*-, and *trans-cis*-nepetalactone, respectively (Fig. 3D). Despite multiple activities in vitro, expression of NEPS1 appeared to be associated primarily with *trans-cis*-nepetalactone production. NEPS5 expression was high in *cis-trans*-nepetalactone producers, suggesting that it is the key *cis-trans* dehydrogenase. However, there was also high NEPS5 expression in a portion of *cis-cis*- and *trans-cis*-producers, suggesting that it might not be dedicated to *cis-trans*-nepetalactone production. NEPS2 was expressed in all plants but was highest in *cis-cis*-nepetalactone producers. This may indicate that it has an as-yet unknown role in this pathway. Curiously, no dehydrogenase was associated with *cis-cis*-nepetalactone production. It is possible that NEPS1 and NEPS5, both expressed at low levels in *cis-cis*-nepetalactone producers, share responsibility for the *cis-cis* dehydrogenation step. However,

Table 1. NEPS and MLPL in vitro activities. Summary of activities observed in in vitro assays with ISY and 8OG (Fig. 3 and figs. S16 to S20). Cyclisation refers to formation of nepetalactol isomers from the reactive ISY product; dehydrogenation refers to formation of nepetalactone isomers from corresponding nepetalactols. Ticks (✓), activity observed; question mark (?), possible activity, not verified; tilde (~), trace activity; double tick (✓✓), in vitro activity supported by in planta gene expression profiling data (only tested for *N. mussinii*).

Enzyme		Cyclization			Dehydrogenation		
		cis-trans	cis-cis	trans-cis	cis-trans	cis-cis	trans-cis
Nm	NEPS1	?			✓	✓	✓✓
Nc	NEPS1	?			✓	✓	✓
Nm	NEPS2						
Nc	NEPS2						
Nm	NEPS3		✓✓			~	
Nc	NEPS3A		✓			✓	
Nm	NEPS3B		✓			~	
Nm	NEPS4			✓✓	✓	?	~
Nc	NEPS4			✓	✓	?	~
Nm	NEPS5	?			✓✓	✓	✓
Nc	NEPS5	?			✓	✓	✓
Nm	MLPL	✓✓					
Nc	MLPLA	✓					
Nc	MLPLB	✓					

the role of *NEPS2* and the missing dedicated cis-cis dehydrogenase remain two unresolved aspects of the nepetalactone biosynthetic pathway.

Evolution of ISY in *Nepeta*

With phylogenetic, genomic, and enzymatic information in-hand, we developed a model of iridoid evolution in *Nepeta* that integrates enzyme and genome evolution. One model for the emergence of metabolic novelty involves an ancestral enzyme with a minor side activity; following gene duplication, this side activity is optimized in one paralog, yielding a novel enzyme with a dedicated biosynthetic role (19, 20). *ISY* is a member of the *PRISE* family, and *N. cataria* and *N. mussinii* contain three different types of *PRISE* homologs: *ISYs*, *P5βRs*, and intermediate sequences that we named secondary *ISYs* (*SISYs*) (Fig. 4, A and B, and fig. S22). *NmSISY* is full length and has low expression levels (fig. S12), while *NcSISYA* and *NcSISYB* are silent, fragmented pseudogenes. *ISYs* are located in the aforementioned gene cluster (hereafter, *NEPS* locus), whereas *P5βRs* and *SISYs* are found as tandem duplicates in a different genomic region (*P5βR* locus) (Fig. 4A and table S7).

To examine how the novel *ISY* gene emerged from a *P5βR* clade in *Nepeta*, we used ancestral sequence reconstruction (ASR) to infer the sequences of *PRISE* genes present at key events in the evolution of the *Nepeta* lineage. ASR has been previously used within the context of plant natural product biosynthesis to investigate the evolution of methyltransferases from promiscuous ancestors (21) and chalcone isomerase from a nonenzymatic ancestor (22). We targeted three key nodes for investigation: *Nepetinae* (*Anc1*), *Nepeta* (*Anc2*), and the *SISY-ISY* duplication (*Anc3*). We used a single reconstruction at each node. These were well supported, with 95, 87, and 80% of codons having a posterior probability above 0.95 for *Anc1*, *Anc2*, and *Anc3*, respectively. *Anc2* has six codons with ambiguous amino acid

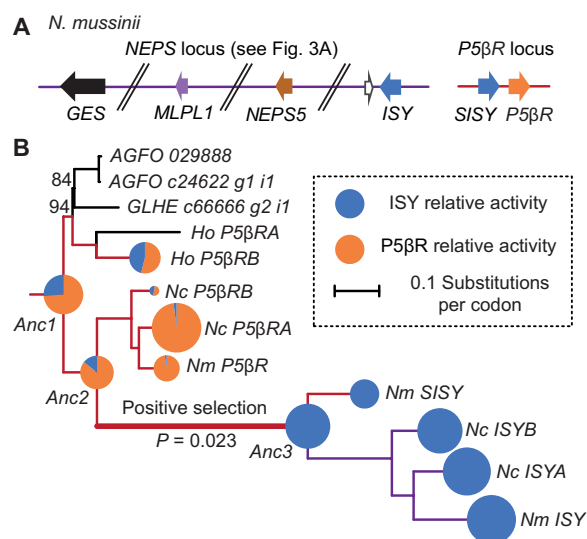


Fig. 4. Evolution of ISY in *Nepeta*. (A) Genomic location of three *PRISE* homologs in *N. mussinii*. Similar genome structures are present in *N. cataria* (table S7 and Fig. 3A). (B) Phylogram of *PRISEs* from *Nepetinae* (subtribe containing *Nepeta*). The highly diverged pseudogenes *NcSISYA* and *NcSISYB* were excluded from the phylogenetic inference to improve model support. Pie charts show in vitro enzyme activities of extant *PRISEs* from hyssop and *Nepeta* and reconstructed ancestral *PRISEs*. For enzyme activities, the area of each chart sector is proportional to relative activity; total chart area is proportional to the sum of relative activities. HoP5βRA failed to express in sufficient quantity to assay. All branches have >99% support unless noted, see fig. S22 for alignment of sequences and fig. S23 for annotated phylogram. Ho, *H. officinalis*; Nm, *N. mussinii*; Nc, *N. cataria*; AGFO, *Agastache foeniculum*; GLHE, *G. hederacea*.

assignments, where the posterior probability of the most likely codon is below 0.6 and the next most likely codon encodes a different amino acid. *Anc3* has just one of these ambiguous positions, and *Anc1* has none.

We measured the catalytic activity of extant and predicted ancestral PRISEs for reduction of progesterone (a putative substrate of P5 β Rs) (23) and 8OG, the substrate of ISY (Fig. 4B, fig. S24, and table S8). Predicted ancestral PRISEs in Nepetinae (*Anc1*) and *Nepeta* (*Anc2*) were capable of catalyzing both reactions. *Anc3*, in contrast, demonstrated no detectable P5 β R activity and a significant increase in ISY activity relative to *Anc2*.

Furthermore, we analyzed the PRISE tree to detect any branches in which genes may have been under positive selection. Selection can be detected by comparing ratios of nonsynonymous (dN) to synonymous mutations (dS) at each codon. Of the five branches investigated (fig. S23 and table S9), positive selection was only detected along the branch from *Anc2* to *Anc3*. Along this branch, 5 of 376 total codons were found to be under selection (dN/dS > 1). Residues identified with particularly significant indications of selection include a lysine to phenylalanine transition (NcISYA position 150, $P = 0.999$), an aspartic acid to lysine transition (NcISYA position 177, $P = 0.944$) and a case where a serine residue had switched codons, via a threonine or cytosine (NcISYA position 86, $P = 0.988$). Recent analysis of the serine codon switching phenomenon indicates that it is driven by selection (24).

Overall, these ancestral reconstructions and positive selection analyses support the model of a gene duplication of a PRISE ancestor with minor ISY side activity, followed by selective pressure to form a dedicated iridoid biosynthetic enzyme. While this hypothesis fits a standard model of enzyme evolution through duplication of promiscuous ancestors, we acknowledge that further work is required to unravel the molecular basis for this transition. More reconstructions at each node would provide greater confidence in the quantitative differences between ancestral activities. Furthermore, mutagenesis experiments would be useful to validate predictions made by both the ASR and positive selection analyses and would, therefore, provide more insight into the evolution of ISY in *Nepeta*.

Assembly of a nepetalactone gene cluster

In addition to the re-evolution of ISY from a PRISE ancestor, the crucial innovation required for nepetalactone biosynthesis was the NEPS enzymes, which act in partnership with ISY to control the profile of stereoisomers formed from the cyclization reaction. These enzymes, despite having diverse cyclase and dehydrogenase activities (Table 1 and Fig. 3), form a single clade that is unique to the *Nepeta* lineage (fig. S25). We compared the evolution and diversification of NEPS with the emergence of ISY activity by generating chronograms of PRISEs and NEPSs (Fig. 5A and figs. S26 to S28).

To account for changes in mutation rates across branches, such as those caused by changing selective pressure, we used a relaxed clock model within a penalized likelihood (PL) framework, which enables each branch to have a separate rate. We also constrained both chronograms at three nodes, including Nepetinae (i.e., the common ancestor of hyssop and *Nepeta*), to gain more accurate divergence time estimates at our nodes of interest.

These chronograms reveal that the most recent common ancestor of the NEPS genes (22 to 18 Ma ago) was present at the time of, or just after, the *Anc2* duplication event (24 to 21 Ma ago). Furthermore, key diversification events of the NEPS genes were concurrent

with the selection and evolution of ISY activity (23 to 9 Ma ago). This timing supports a model where ISY and NEPS catalytic activities coevolved.

It is possible to infer the genomic location of the ancestral PRISE genes and thereby address whether gene clustering preceded or followed evolution of nepetalactone biosynthesis. Given the location of extant SISYs and P5 β Rs at the P5 β R locus (Fig. 4A and table S7), we can infer that PRISE ancestors *Anc1*, *Anc2*, and *Anc3* were also located in this locus (Fig. 5A). Approximately 23 Ma ago, *Anc2* at the P5 β R locus underwent tandem duplication and neofunctionalization; one descendant maintained P5 β R activity, leading to extant P5 β Rs, while the other acquired ISY functionality through positive selection leading to *Anc3* (Fig. 5B). Concurrent with this *Anc2* duplication event, within the NEPS locus, the NEPS common ancestor underwent a series of gene duplications. The ISY-like *Anc3* then duplicated into the NEPS locus via a dispersed duplication (e.g., transposition or translocation, 9 Ma ago). The original copy of *Anc3* at the P5 β R locus became redundant, leading to reduction of expression and eventual pseudogenization, as observed in the form of SISY in current *N. mussinii* and *N. cataria* genomes. Thus, evolution of ISY activity occurred before the formation of the gene cluster (Fig. 5B).

The speciation of both *N. mussinii* and *N. cataria* occurred after gene cluster formation (i.e., the movement of ISY into the NEPS locus), as supported by the presence of the gene clusters and evidence of tandem SISY/P5 β R in the *N. mussinii* genome and both *N. cataria* subgenomes, indicating a common ancestor with these features. A comparison of species and gene divergence times also supports a chronology where speciation (~5.5 Ma ago) (fig. S26) succeeded the ISY clustering (~9 Ma ago) (Fig. 5A).

The location of *GES* also supports a chronology where evolution of enzyme activity precedes gene cluster formation. In *N. mussinii*, the functional *GES* is clustered with ISY and NEPS in the NEPS locus, while a pseudogenized *GES* is present at a different locus (table S10). The equivalent syntenic loci in *N. cataria* contain functional *GES*s, suggesting that in the *N. mussinii* lineage (i.e., after speciation of *N. cataria* and *N. mussinii*), a functional *GES* moved into the NEPS/ISY gene cluster.

Through a simultaneous examination of enzyme and genome evolution, it is possible to provide insight into the formation and divergence of plant metabolic gene clusters. In particular, this study of *Nepeta* iridoid clusters highlights how biosynthetic genes were recruited into a gene cluster after they gained function. This chronology of clustering following functionalization has previously been proposed in the evolution of other plant metabolic gene clusters (25, 26). In the *Nepeta* genomes, the presence of the pseudogenized SISYs and *GES* provides clear experimental evidence supporting this mechanism of cluster formation.

DISCUSSION

The evolution of nepetalactone biosynthesis in *Nepeta* is not simply a re-emergence of iridoid biosynthesis in this lineage; it also represents an evolutionary innovation. Nepetalactone is an example of repeated evolution with a twist; while nepetalactones maintain the iridoid structure, there are key differences compared to other iridoids found in the mint family. Most notably, NEPS1 and NEPS5 oxidize the lactol of the ISY product to form lactone, while iridoids in the rest of the mint family are glucosylated at this position (Fig. 1A).

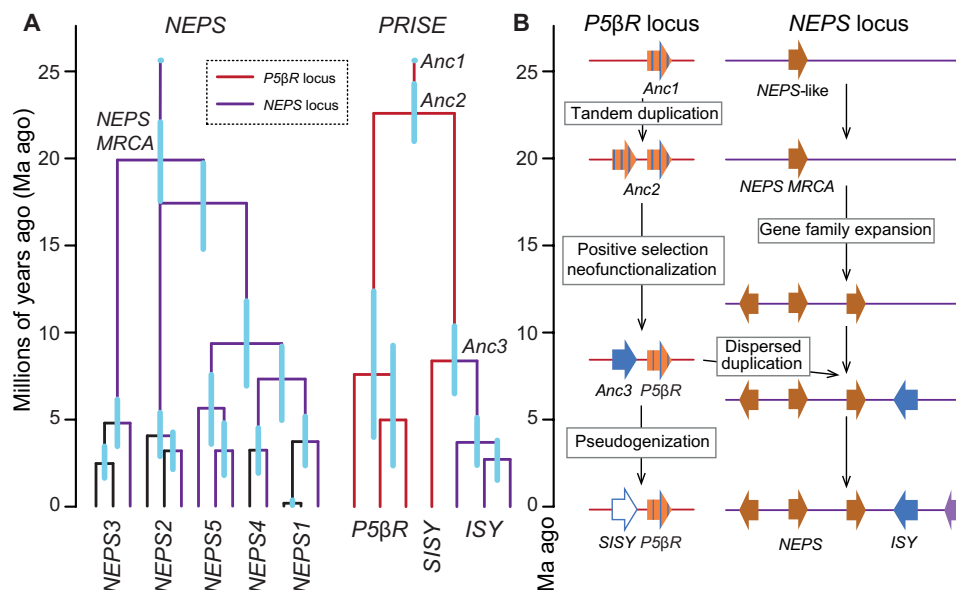


Fig. 5. Enzyme and genome evolution in *Nepeta* iridoid biosynthesis. (A) Selected *Nepeta* clades from chronograms of *NEPS* and *PRISE* genes. Blue bars are 95% confidence intervals. Colored branches represent genomic location. Complete chronograms can be found in figs. S27 and S28. (B) Proposed chronology of events in *Nepeta* nepetalactone biosynthesis evolution.

Thus, nepetalactone iridoids in *Nepeta* function as volatiles rather than the two-component defense role adopted by glycosylated iridoids (12). In addition, while the rest of the Lamiaceae produce only a single iridoid scaffold stereoisomer, NEPS3 and NEPS4 allow *Nepeta* to produce different ratios of nepetalactone stereoisomers, which results in changes to the insect repellent properties (4). Many non-iridoid volatile monoterpenes (such as 3-pinane produced in hyssop) demonstrate general insect repellent properties (27). Nepetalactone is produced de novo by aphids as a sex pheromone (28); thus, its production by *Nepeta* may mediate as-yet unknown interactions with aphids (29). Such a scenario could account for the strong selective pressure required for the evolution of nepetalactone biosynthesis, which represents an important future topic of research.

Nepeta also produces glycosylated iridoids including 1,5,9-epideoxyloganic acid and nepetaside (figs. S5 and S6). While it is unclear when these iridoids emerged in *Nepeta* relative to the nepetalactones, ISY activity is required for their formation. Biosynthesis of these *Nepeta*-specific iridoid glycosides may also require the activity of NEPS: Nepetaside has a lactone moiety, which points to dehydrogenase activity, and 1,5,9-epideoxyloganic acid has *cis-cis* stereochemistry, indicating the involvement of a cyclase. This suggests that *Nepeta* iridoid glycoside biosynthesis requires both ISY and NEPS and therefore may have arisen during, or soon after, the emergence of nepetalactones. Further elucidation of glycoside biosynthesis in *Nepeta* is required to test this hypothesis.

The biosynthesis of the iridoid cat attractant nepetalactone in *Nepeta* provides a rich system for investigation of the dynamics of metabolic and chemical defense evolution. The loss of iridoid biosynthesis in the early evolution of the mint subclade Nepetoideae appears to be due to the interplay of regulatory changes (reductions in expression of upstream genes) and gene loss (deletion of ISY). Its re-emergence in *Nepeta* appears to have been driven by the coevolution of ISY and NEPS, with chronograms that date the divergences of *PRISEs* and *NEPSs* genes consistent with the timing required for this

model. The presence of pseudogenes, in combination with phylogenetic analyses, ASR, and selection analyses together provide a molecular snapshot indicating that the evolution of iridoid biosynthesis in *Nepeta* preceded the formation of the iridoid gene cluster. This proposed chronology suggests that gene clusters are not the cradle of plant metabolic novelty but may instead emerge subsequent to enzyme evolution while the nascent metabolism is under strong positive selection. This study highlights the complementarity of enzyme and genome evolution in elucidating the emergence of novel chemistry in plants.

MATERIALS AND METHODS

Tissue metabolite analysis by GC-MS

For metabolite analysis of tissues by gas chromatography–mass spectrometry (GC-MS), two approaches were taken. Internal pools of volatiles were analyzed after their extraction from a tissue by dichloromethane as described previously (10). Compound identification was achieved using electron impact (EI) spectra, picking best-matched compounds in the National Institute of Standards and Technology Standard Reference Database EI library. Identification of nepetalactone isomers in *Nepeta* tissues was performed as previously described (7). The proportions of nepetalactone isomers present was determined by identifying nepetalactone peaks using verified standards and then dividing isomer peak area by total nepetalactone peak area.

Extraction and analysis of iridoid glycosides by liquid chromatography–MS

Frozen tissues were homogenized using a TissueLyser II (Qiagen, UK), and 50 mg of the homogenate was suspended in 1 ml of methanol. Samples were extracted by vortex for 2 min followed by ultrasonication in a bath at room temperature for 5 min. For each tissue, three extracts were collected from the same biological tissue. The extracts were centrifuged and diluted with aqueous formic acid (0.1%, v/v and 1:5, v/v). Last, the supernatant was filtered through a hydrophilic

polytetrafluoroethylene (PTFE) 0.22- μm membrane (Merck, Feltham, UK) for nontargeted tandem mass analysis using high-resolution MS.

Shimadzu IT-ToF-MS (ion-trap time-of-flight mass spectrometer) was used to analyze the extracts. Identification and chromatographic separation of the compounds on this instrument were performed on a Shimadzu Nexera X2 UPLC system (Shimadzu Corp., Kyoto, Japan). Each sample (4- μl injection) was eluted through a Kinetex XB-C18 2.6- μm column (100 mm by 2.1 mm, 100 \AA ; Phenomenex, UK) at a column temperature of 40°C and a flow rate of 0.5 ml min⁻¹. The mobile phase consisted of (A) aqueous formic acid (0.1%, v/v) and (B) acetonitrile. A linear gradient used was as follows: 0 to 10 min, 26% B; 10 to 11 min, 26 to 95% B; 11 to 12 min, 95 to 2% B; 12 to 15 min, 2% B. Optimized MS conditions were as follows: negative ion mode; negative electrospray voltage, -3.5 kV; CDL (curve desolvation line) temperature, 250°C; block heater temperature, 300°C; nebulizing gas (N₂) flow, 1.5 liter min⁻¹; drying gas (N₂) pressure, 100 kPa. Full-scan MS (mass spectrum) readings were acquired in the mass/charge ratio (*m/z*) range of 100 to 1200 for MS and *m/z* 100 to 1000 for MS². The MS² data were collected in an automatic data-dependent manner using collision-induced dissociation of the most abundant singly charged species in a scan, with an exclusion time of 0.8 s. Argon was used as the collision gas, and the collision energy was set at 50%. Before data acquisition, the instrument was calibrated with sodium trifluoroacetic acid clusters (CF₃CO₂Na) against the entire mass range (*m/z* 100 to 1200 Da) specified for the instrument. Data acquisition and processing were performed using LCMSSolution (version 3.80, Shimadzu Corp., Kyoto, Japan).

The occurrence of iridoid glucosides was tentatively confirmed by qualitative analysis using a combined set of criteria. This included retention time (chromatographic separation), accurate mass spectra, tandem mass [loss of hexose sugar: $\Delta 162$ and other characteristic iridoid fragments (30)], and photodiode array. All major chromatography peaks with a signal-to-noise ratio of 3:1 or higher that could be recognized as iridoid glucoside/s were taken into consideration. The results were compared with previous reports for isolation and spectral identification of iridoid glucosides from the studied species (31).

Genome sequencing, assembly, and annotation

DNA was extracted from young leaves of *N. cataria*, *N. mussinii*, and *H. officinalis* using the Qiagen DNeasy Plant Mini Kit or with a modified cetyl trimethylammonium bromide (CTAB) method (32). For each species, multiple Illumina-compatible paired-end libraries and mate-pair libraries were constructed and sequenced on the Illumina platform as previously described (tables S1 and S2) (33). Paired-end reads were cleaned by removing adapters and low-quality sequences using Cutadapt (34), while mate-pair libraries were processed using NextClip (35). ALLPATHS-LG (v52488) (36) was used to generate an assembly of each genome. For *H. officinalis*, chromosome-scale assemblies were generated using Proximo Hi-C scaffolding as described previously (37), and gaps were filled using PBjelly (v15.8.24) (38) with reads greater than 1 kb. The gap-filled pseudomolecules were error-corrected using the Illumina whole-genome shotgun sequencing reads with Pilon (v1.22) (39). Genome assembly quality was assessed using Benchmarking Universal Single-Copy Orthologs v3.0.2 (40); final metrics of the three assemblies including quality assessment results demonstrate high-quality assemblies for these three species (table S3).

Genomes were annotated for repetitive sequences and protein-coding genes as described previously (41). Briefly, custom species-

specific repeat libraries were constructed using RepeatModeler (v1.0.8; <http://repeatmasker.org/>), and putative protein-coding genes were removed using ProtExcluder (v1.1) (42). RepeatMasker (v4.0.6) was used with the custom species-specific repeat libraries in addition to Viridiplantae RepBase (43) repeats to mask the cognate genome. To provide transcript evidence for annotation, *N. cataria*, *N. mussinii*, and *H. officinalis* were grown in growth chambers until plants reached maturity. Diverse tissues (closed flower buds, open flowers, immature leaf, mature leaf, petiole, root, and stem) were collected from each species. Total RNA was isolated, treated with TURBO DNA-free DNase (Thermo Fisher Scientific, Waltham, MA), libraries were constructed using the Illumina TruSeq Stranded mRNA Library Preparation Kit (Illumina, CA) and sequenced on the Illumina platform generating paired-end 150-nt reads. Reads were cleaned using Cutadapt (v1.15) (34), aligned to the cognate genome using TopHat2 (v2.1.1) (44), and genome-guided transcript assemblies were generated using Trinity (v2.6.6) (45). Species-specific genome-guided leaf RNA-sequencing (RNA-seq) assemblies were used to train Augustus (v3.1) (46). Gene structures were improved using additional genome-guided transcript assemblies using PASA2 (v2.0.2; <https://github.com/PASApipeline>) (47) generating a set of working models. Expression abundances [fragments per kb exon model per million mapped reads (FPKM)] were determined from the TopHat2 alignments using Cufflinks2 (v2.2.1; table S4) (48). Functional annotation of the gene models was determined using BLAST search results against the predicted *Arabidopsis thaliana* proteome (TAIR10; Arabidopsis.org), Swiss-Prot entries (release 2015_08), and Pfam search results were generated using HMMER v3.1b2 (49) with a cutoff of 1×10^{-5} . From the working gene models, a high confidence gene set was identified on the basis of expression in any RNA-seq library greater than 0 FPKM or that had a match to a Pfam domain. Partial gene models and models with matches to transposable element-related PFAM domains were excluded from the high confidence model set.

Identification of syntenic loci

All-versus-all BLASTP of the predicted proteins was performed with BLAST+ (v2.7.1) with an E-value cutoff of 1×10^{-5} and a maximum of five alignments reported. MCScanX (git commit 7b61f32) (50) was run with the default parameters to generate putative collinear blocks that were refined with manual curation using the BLASTP results.

N. mussinii diversity panel

Different accessions (genotypes) of *N. mussinii* were obtained from Herbal Haven (Saffron Walden, UK) and maintained in glasshouses. To determine the chemotype of each accession, plants were cut back, and after 2 weeks, young leaves were isolated. Three samples, each from different branches, were taken from each plant. Leaf tissue (approximately 100 mg) was frozen in liquid nitrogen, homogenized with a ball mill with a tungsten bead (27 Hz, 30 s, two repetitions) and then split for parallel RNA isolation and metabolite profiling.

Nepetalactone stereoisomer content was analyzed by GC-MS as described previously (7). In all samples, there was a single isomer accounting for >60% of nepetalactone content, and this major isomer was used to define the sample chemotype.

Total RNA was extracted using a standard CTAB protocol (51), and RNA-seq libraries constructed and sequenced as described above with the exception that single-end 50-nt reads were generated (table S6). Reads were cleaned using Cutadapt (v1.14) (34) and aligned

using TopHat2 (v2.1.1) (44) to the *N. mussinii* reference genome appended with the previously reported *NmNEPS3* sequence (9); expression abundances were calculated using Cufflinks (v2.2.1) (48). To provide comparable expression abundances from the gene expression atlas of the reference genotype used for assembly and annotation, 50 nt from read 1 of the *N. mussinii* reference gene expression atlas paired-end reads (see above) was clipped using Cutadapt (34) and processed in parallel with the *N. mussinii* diversity panel libraries.

Gene expression analysis

Unless otherwise stated, the expression matrix in FPKM was log-transformed using the formula $\text{Log}_2(\text{FPKM} + 1)$, and analyses were made using the *stats* library in the R platform (52). For examination of *N. mussinii* diversity panel, analysis of variance models was used to fit log-transformed expression levels [$\text{log}_2(\text{FPKM} + 1)$] for every gene across the three different chemotype categories. Tukey's test followed by Benjamini-Hochberg multiple test correction was then used to identify *P* values for each comparison. Correlations between *cis-trans*-nepetalactone, *MLPL*, and *NEPS5* were further examined using Spearman's rank correlation.

Self-organizing maps (SOM) were performed on the Z-scores of the log-transformed expression matrix using the *som* function in the *kohonen* library (53). The Z-score was calculated by subtracting the mean expression of each gene and dividing by their SD, resulting in each gene having a mean expression of 0 and an SD of 1. To avoid boundary effects, the SOM was set to have a 20×20 toroidal grid, with a hexagonal topology. To determine internodal similarity, the codebook vectors of the nodes were clustered via hierarchical clustering, and enrichment of biosynthetic genes in the selected cluster was calculated using a hypergeometric test. Tissue-specific expression patterns were analyzed and presented using hierarchically clustered heatmaps, using the *heatmap* library (54). For both internodal clustering in SOMs and heatmaps, hierarchical clustering followed a complete linkage method of Euclidean distances.

Identification and cloning of genes

Genes of interest were identified by blast searching gene models with previously characterized iridoid biosynthesis enzymes from *Nepeta* (NEPSs and PRISEs) and *Catharanthus* (GES, G8H, and HGOA) (5, 7, 9, 10). The genomic locations and tissue expression patterns of the genes were used to assess whether the genes were genomically clustered and/or coexpressing with other iridoid biosynthetic genes.

Physical complementary DNA libraries were formed from young leaf RNA using SuperScript IV Reverse Transcriptase (Thermo Fisher Scientific) with oligo d(T)₂₀ primers according to kit instructions. Genes were cloned into pOPINF *Escherichia coli* expression vectors as previously described (9), with the exception of G8Hs which were cloned into a pESC-Leu2d vector for expression in yeast (55). Genes with closely related homologs were first cloned using unique UTRs (untranslated regions), and thereafter, the coding region was amplified for addition to the expression vector. PRISE and GES genes were obtained as N-terminal truncates to improve soluble expression. Predicted ancestral sequences, along with selected genes that could not be cloned or recombinantly expressed, were obtained via synthetic genes (Twist BioScience). Synthetic genes were codon-optimized for *E. coli* using COOL (56), optimizing for codon context and GC content. Synthetic genes were subcloned from the shuttle vector (pTwist Amp High Copy) into pOPINF, except NcNEPS4 which

was provided in a pET28(+) expression vector and used directly. Hyssop GES and HGOA did not express in pOPINF and were cloned into pOPINJ (glutathione S-transferase tag) to improve protein solubility but did not express with this plasmid either.

All cloned and subcloned genes were sequenced by Sanger Sequencing (Eurofins Genomics). A few nucleotide differences were observed between genomic and cloned sequences.

Enzyme expression and purification in *E. coli*

For expression of NEPSs and MLPLs, *E. coli* expression strain cells (SoluBL21) containing the plasmids of interest were grown overnight [LB medium, 10 ml, with carbenicillin (100 µg/ml)]. 2xYT medium [100 ml, with carbenicillin (100 µg/ml)] was inoculated with overnight culture (5%, v/v) and grown at 37°C until OD₆₀₀ (optical density at 600 nm) = 0.5. The culture was then grown at 18°C until OD₆₀₀ = 0.6 to 0.8, and protein production was induced with addition of isopropyl-β-D-thiogalactopyranoside (500 µM). The cells were incubated at 18°C for 16 hours before harvesting by centrifugation (4000g, 10 min). If the pellets were not used immediately, they were washed in phosphate-buffered saline before storage at -20°C.

Cell pellets were resuspended in BugBuster MasterMix [10 ml, with cOmplete EDTA-free protease inhibitors (Roche)], incubated at 4°C for 20 min, and then centrifuged (35,000g, 20 min). Ni-nitrilotriacetic acid agarose (1 ml; Qiagen) was washed in binding buffer [50 mM tris-HCl (pH 8), 50 mM glycine, 5% (v/v) glycerol, 0.5 M NaCl, 20 mM imidazole, and 1 mM dithiothreitol (DTT)] and added to the supernatant lysate, and the mixture was incubated at 4°C for 1 hour, gently rocking. The mixture was centrifuged (1000g, 1 min), and the supernatant was discarded. The Ni-NTA pellet was washed three times with 10 ml of binding buffer, and then, elution buffer [50 mM tris-HCl (pH 8), 50 mM glycine, 5% (v/v) glycerol, 0.5 M NaCl, 500 mM imidazole, and 1 mM DTT] was added (2.5 ml). The mixture was centrifuged (1000g, 1 min), and the supernatant was collected and filtered. The buffer was exchanged with sample buffer [20 mM Hepes (pH 7.5) and 150 mM NaCl] using a PD-10 column (GE Healthcare). The proteins were aliquoted, flash-frozen in liquid nitrogen, and stored at -80°C. SDS-polyacrylamide gel electrophoresis and spectrophotometric analysis (absorbance at 280 nm) were used to check purity and approximate quantity of protein.

NmNEPS4 and NcNEPS4 were grown as in 1 liter of cultures and purified by ÄKTA as previously described (6). HGOA and GES were purified as described above but with 1 liter of cultures and lysis by sonication (2 min total, 2 s on, 3 s off; amplitude, 40% pulses; Sonics Vibra-Cell). PRISEs were obtained as described above but in 1 liter of culture, with lysis by cell disruption (two passes, 25 kPi, Constant Systems) and four buffer exchanges using centrifugal filtration [Amicon Ultra 10-kDa molecular weight cutoff (Merck)]. Of the PRISE proteins examined, only HoP5βRA failed to express in adequate quantities for activity assays. GES and HGOA from hyssop failed to express adequately for enzyme assays, despite attempts to optimize conditions.

GC-MS general method

For GC-MS analysis of enzyme assays, samples were injected in split mode (2 µl; split ratio, 5:1) at an inlet temperature of 220°C on a Hewlett Packard 6890 GC-MS equipped with a 5973 mass selective detector and an Agilent 7683B series injector and autosampler. Separation was performed on a Zebron ZB5-HT-INFERNO column (5% phenyl methyl siloxane; length, 35 m; diameter, 250 µm) with

guard column. Helium was used as mobile phase at a constant flow rate of 1.2 ml/min and an average velocity of 37 cm/s. Two temperature runs were used for detection: Method 1 (GES, G8H, and NEPS assays): After 5 min at 80°C, the column temperature was increased to 110°C at a rate of 2.5 K/min then to 280°C at 120 K/min and kept at 280°C for another 4 min. Method 2 (HGOA assays): After an initial temperature at 60°C, the column temperature was increased to 100°C at a rate of 20 K/min then to 160°C at 2 K/min, then another increase to 280°C at 100 K/min, and maintained for 4 min. A solvent delay of 5 min was allowed before collecting MS spectra at a fragmentation energy of 70 eV. Chemically characterized standards were used to identify compounds by retention time and EI spectra.

End-point enzyme assays

End-point assays using 8OG as a substrate were performed as described previously (6). For assays with ISY, NEPS, and MLPL (100 μ l): buffer [0.1 M 3-(*N*-morpholino)propanesulfonic acid (MOPS) (pH 7.5)], ISY (250 nM), NEPS/MLPL/BSA (typically 2 μ M each unless noted), NAD⁺ (5 mM, added in the presence of NEPSs), NADPH (1 mM), and 8OG (0.5 mM, added last) were mixed and incubated for 3 hours at 30°C. The reactions were extracted into 100 μ l of ethyl acetate [with 1 or 10 μ M (+)-camphor internal standard], and the organic fraction was analyzed by GC-MS.

For quantification, GC-MS chromatograms were analyzed using OpenChrom Lablicate Edition (version 1.4.0.202001031827). Peaks were detected using Peak Detector First Derivative tool and integrated using Peak Max Integrator. Peaks of interest were identified by comparing retention times and EI spectra to chemical characterized standards. Peak areas were normalized across runs using the (+)-camphor internal standard and presented as areas relative to 1 μ M camphor.

Activity of purified GES was determined by incubating GES (4.43 μ M), DTT (1 mM), MgCl₂ (20 mM), MnCl₂ (500 μ M), glycerol (10%, v/v), geranyl pyrophosphate (0.1 mM), and MOPS buffer (10 mM, 100 μ l total) at 30°C for 1 hour. Activity of purified HGOA was determined by incubating enzyme (7 μ M), NAD(P)⁺ (2 mM), 8-hydroxygeraniol (0.5 mM), NaCl (25 mM), and Hepes buffer (12.5 mM, 100 μ l total) at 30°C. Reactions were quenched by mixing 100 μ l of ethyl acetate, centrifuging to separate and collecting the top organic layer for analysis by GC-MS.

Activities of G8H enzymes were determined using yeast feeding assays. *Saccharomyces cerevisiae* (pep4KO) cells containing the appropriate vectors were used to inoculate 2 \times 2 ml of SC-Leu media with 2% (v/v) glycerol. Cultures were incubated for 48 hours at 30°C, pooled, and then pelleted at 3500g for 5 min. The cultures were washed twice with 10 ml of water, pelleting each time at 3500g for 5 min. SC-Leu (2 ml) with 2% (v/v) galactose was added to each culture, which was then split into four tubes. To three of these aliquots, 0.5 mM of geraniol was added, and to one, an equal volume of analytical grade ethanol was added. The aliquots were incubated for 24 hours at 30°C. Reactions were quenched by adding 200 μ l of 3:1 ethyl acetate:acetone solution. The mixture was vortexed and centrifuged, and the top organic layer was collected and filtered for GC-MS analysis.

PRISE activities

Progesterone 5 β -reductase activities were measured as initial rates using GC-MS. Reactions (400 μ l total, $n = 3$ per enzyme) consisted of enzymes (500 nM), NADPH (1 mM), progesterone (400 μ M), dimethyl sulfoxide (4%, v/v), and MOPS buffer [20 mM (pH 7.5)].

Components were mixed and incubated at 30°C. Samples (100 μ l) were taken from reactions at 2 and 4 hours, extracted into ethyl acetate (100 μ l), and analyzed by GC-MS (see method below). Total ion chromatograms were analyzed Agilent MassHunter Qualitative analysis. Product peaks were identified by retention time comparison to an authentic standard (5 β -dihydroprogesterone) and integrated. Peak areas were converted to concentrations using a product standard curve, and initial linear rates were calculated for each replicate. Analysis of variation was used to compare activities across enzymes (log₁₀ transformation, “aov” function in R), and results were grouped using Tukey’s post hoc test ($\alpha = 0.05$, “HSD.test” function in R).

ISY activities were measured on a FLUOStar Omega multiplate reader (BMG Labtech) using plate kinetics mode and absorbance at 340 nm (25°C, positioning delay 0.2 s, 22 flashes per well). Reactions (200 μ l total) consisted of enzymes (5 to 300 nM), NADPH (100 μ M), 8OG (0 to 100 μ M), and MOPS buffer [20 mM (pH 7.5)]. Components were preincubated for 2 min before the addition of 8OG and then mixed by pipetting. NADPH consumption was measured, and the initial linear rate was calculated (1 to 20 min, “lm” function in R). For activity measurements (100 μ M 8OG, $n = 3$ to 6 per enzyme), analysis of variation was used to compare activities across enzymes (log₁₀ transformation, “aov” function in R), and results were grouped using Tukey’s post hoc test ($\alpha = 0.05$, “HSD.test” function in R). For kinetic analyses (0, 1.5625, 3.125, 6.25, 12.5, 25, 50, or 100 μ M 8OG, $n = 21$ to 32 per enzyme), the Michaelis-Menten or substrate inhibition models were fit to rates (“nls” function in R).

For pie chart depiction of PRISE activities, mean values were calculated for each enzyme and then normalized by dividing means by the maximum observed rates (ISY activity = NmISY and P5 β R activity = NcP5 β RA). The area of each pie chart section is proportional to the normalized activity, and thus, the total area of each chart is proportional to the sum of the two normalized activities.

Early iridoid gene phylogenetics

For early iridoid enzymes, genes of interest were identified using previously characterized iridoid biosynthesis enzymes from *Catharanthus* (*GES*, CRO_T119458; *G8H*, CRO_T133061; *HGOA*, CRO_T107879) (7). Lamiaceae orthogroups containing the *Catharanthus* genes of interest were identified (*G8H*, OG0000115; *GES*, OG0011057; *HGOA*, OG0003405) (10). Genome gene models for *Hyssopus* and *Nepeta* were searched by blast for related sequences. Near-identical and fragments of sequences were removed from the analysis. Open reading frames were extracted, aligned by translation using MAFFT (Auto settings, v 7.388) (57), and phylogenies were inferred from codons using iQTree v1.6.9 (58) with ModelFinder (59) together with UFBoot2 ($\times 1000$) (60) and SH-aLRT supports ($\times 1000$). Outgroups were selected on the basis of known species relationships. For *G8H*, the phylogeny of the large orthogroup was initially inferred using FastTree (61) before the clade most closely related to the specified *Catharanthus* *G8H* sequence was identified. The expression patterns of *Nepeta* genes of interest were used to identify which genes are most likely involved in iridoid biosynthesis. Phylograms were depicted using Geneious Prime 2019 or iTOL 4.4.2 (62).

PRISE phylogenetics

Sequences corresponding to PRISE homologs were obtained through orthogroup analysis of Lamiaceae and reference transcriptomes (OG0002182) (10). Homologs were identified from the *Nepeta*

and *Hyssopus* genomes by blast searching gene model coding sequences. The *NcSISYB* pseudogene did not appear in the gene models. To identify *NcSISYB*, *NmSISY* was used as a query to blast the *N. cataria* genome sequence. The reversed sequence in the region of g3325 had notable sequence similarity with the 5' region of *NmSISY* and *NcSISYA*. There also appeared to be some sequence similarity with the 3' of *NcSISYA* downstream of a string of NNNs adjacent to g3324. This region appears to be a *SISY* pseudogene, *NcSISYB*.

Extra *PRISE* sequences were identified by blast searches of National Center for Biotechnology Information (NCBI) nr databases, *Mentha* transcriptomes (<http://langelabtools.wsu.edu/mgr/>), sequence read archive (SRA) Lamiaceae transcriptomes, and “skim” genomes. For SRA-derived transcriptomes, raw reads were downloaded from NCBI SRA for *Isodon rubescans* (SRR714241), *Ocimum americanum* (SRR2029848 and SRR2029849), *Ocimum teniflorum* (SRR1177846), *Phlomis purpurea* (SRR1920173), *Salvia miltiorrhiza* (SRR1745640), and *Salvia sclarea* (SRR983807). Adapters and low-quality bases were removed using Cutadapt (v1.8.1) (34) requiring a minimum base quality of 20 and a minimum size of 20 nt. De novo transcript assemblies were generated using Trinity (v20140717) (45) using the default parameters, and only transcripts with length equal and greater than 150 base pairs (bp) were retained for subsequent analyses. For generation of skim genomes for *Agastache foeniculum*, *Melissa officinalis*, *Perilla frutescens*, *Lycopus americanus*, *Glechoma hederacea*, and *Collinsonia canadensis*, approximately 30 million 2 × 150 bp reads were generated for each mint species using the HiSeq 4000 platform. Adapters and low-quality bases were removed using Cutadapt (v1.8.1) requiring a minimum base quality of 20 and a minimum size of 20 nt. De novo genome assemblies were generated using Abyss (v1.9.0) with a kmer size of 65 (63).

Open reading frames for *PRISE* enzymes were extracted from the transcripts, and stop codons were removed. Near-identical sequences were removed from the analysis. Sequences ROMY_c75305_g1_i2 and PRMI_c25272_g1_i1 were obtained by searching raw isoform transcriptomes (10). A sequence labeled ORVU_c87504_g1_i1 was removed from the analysis as it was revealed to be a contamination from ROMY_c75305_g1_i2. *NcSISYA* and *NcSISYB* were not included in the analysis, because their inclusion caused instability in the tree topology. For *PRISE* genes from *Nepeta*, the sequenced verified cloned gene sequences were used in phylogenetic analysis. For *hyssop* *PRISEs*, the original genomic sequences and not the cloned gene sequences were used in the phylogenetic analyses, as this analysis was performed before cloning of these genes.

Translated sequences were aligned using MAAFT (G-INS-i, v7.017) (57). The codon-based phylogeny was inferred using iQTree v1.6.1 (58) with ModelFinder (59). The output tree was then used to realign the codon sequences using PRANK (64) before the phylogeny was inferred again using IQ-TREE v1.6.1 with ModelFinder together with ultrafast bootstraps (UFBoot2, ×1000) (60) and SH-aLRT supports (×1000). The cladogram was depicted using the iTOL 4.4.2 (62) and Adobe Illustrator.

Ancestral sequence reconstruction

For prediction of ancestral sequences and analysis of positive selection, a *PRISE* subtree was isolated with PEVO_c56018_g1_i3 as an outgroup. Short sequences (<1159 nucleotides) were removed, and the phylogeny was again inferred using iQTree v1.6.9 with ModelFinder together with UFBoot2 (60) (×1000) and SH-aLRT supports (×1000).

This tree was used for ASR with FastML using default codon settings (65). For *Anc1* and *Anc2*, the most probable sequences were selected for protein assays. For *Anc3*, the most probable sequence was used with the exception of codon 283. The amino acid at codon 283 is equivocal: p(TTG, Leu) = 0.38 and p(TTC, Phe) = 0.34. The *Anc3* used had a TTC (Phe) in this position, as it was based on a preliminary iteration of the gene phylogeny. Phe is present in this equivalent position in *Anc1*, *Anc2*, and *Nepeta* P5BRs, whereas Leu is present in all *Nepeta* ISYs. Therefore, the presence of Phe-283 in the tested *Anc3* is very unlikely to be responsible for its ISY-like nature. For expression and protein production in *E. coli*, sequences were truncated (starting at S/NVAL) and codon-optimized.

Positive selection analysis

The focused *PRISE* gene phylogeny used for ASR was also used for positive selection analysis using PAML 4.9i (66). The CodeML software implemented in PAML can test for positive selection in codon alignments along gene lineages and in specific sites. This is achieved by modeling ratios of synonymous mutation rates to nonsynonymous mutation rates ($d_N/d_S = \omega$). First, branch lengths were optimized using the M0 model (single ω across alignment and phylogeny) with codon model 2 (F3X4). These branch lengths were used as initial values to fit a variety of different codon models to the data using the M0 model. A total of 11 codon models were tested (parameters: CodonFreq = 0, 1, 2, 3, 6, or 7 and estFreq = 0 or 1) and compared using Bayesian information criteria (BIC) ($n = 376$, number of informative codon patterns). The fMutSel codon model with observed codon frequencies (CodonFreq = 7, estFreq = 0) was the best fit according to BIC and was used for positive selection tests (67).

The branch-site model A test 2 was used to detect positive selection along specified branches in the phylogeny (parameters: model = 2, NSites = 2). For H_0 , ω_2 for the selected branch is fixed at 1 (fix_omega = 1, omega = 1), whereas for H_1 , ω_2 is estimated (fix_omega = 0). A likelihood ratio test was used to determine whether $\omega_2 > 1$ is significant (positive selection). Five separate branches were tested for positive selection, and the *P* values were corrected using Benjamini-Hochberg adjustment.

NEPS sequences and phylogenetics

Sequences corresponding to *NEPS* and *NEPS*-like homologs were obtained through orthogroup analysis of Lamiaceae and reference transcriptomes (OG0004576) (10). *NEPS* and *NEPS*-like genes within *Nepeta* and *hyssop* were identified by blasting gene models (blastn) with *NcNEPS1* and *NmNEPSL1* (g21780). As described above for the *PRISEs*: published transcriptomes, SRA-derived transcriptomes, and skim genomes were queried to identify more *NEPS* homologs identified. Open reading frames were identified, and short sequences were removed (<580 bp). Sequences were aligned (translation align, MAAFT) (57), and a maximum-likelihood tree was inferred (iQTree) (58). The clade containing *NEPS* and *NEPS*-like sequences was subsampled, keeping a sequence from *Catharanthus* as an outgroup (CRO_T131109). The codon sequences were realigned with PRANK (64), and the tree was inferred with iQTree (58).

To check thoroughly for *NEPS* genes outside *Nepeta*, *NcNEPS1* was used as a query to blast (blastn) other databases. Reasonable blast hits (>50% coverage, >60% pairwise identity) were obtained, aligned with MAAFT to *NEPS* and *NEPS*-like genes from the Lamiaceae, and a tree was inferred using FastTree (61). The placement of the sequences within the phylogeny was used to determine whether

these sequences were within the *NEPS* clade or were merely *NEPS*-like sequences from the wider SDR110C family. Numerous databases were searched: *Callicarpa americana* (gene models, unpublished from Mint Evolutionary Genomics Consortium); *Salvia hispanica* (contigs, unpublished from Mint Evolutionary Genomics Consortium); hyssop (genome, presented here); *Mentha longifolia* (genome scaffolds); *S. miltiorrhiza* (genome scaffolds); skim genomes as described above for *A. foeniculum*, *M. officinalis*, *P. frutescens*, *L. americanus*, *G. hederacea*, and *C. canadensis* (unpublished, from Mint Evolutionary Genomics Consortium); *Tectona grandis* (chromosome assembly) and *Dracocephalum tanguticum* (reads identified by blast searching NCBI SRA). No databases other than those from *Nepeta* contained sequences which placed phylogenetically within the *NEPS* clade, indicating that *NEPS* evolved within the lineage of *Nepeta* or, more strictly, along the stem lineage from the Nepetinae common ancestor to the last common ancestor of *N. mussinii* and *N. cataria*.

Molecular dating analyses

We identified the largest subclades in each of our *PRISE* and *NEPS* ML trees (figs. S22 and S28) that could be reliably rooted with at least one outgroup sequence from Lamiales. Sequences comprising these *PRISE* and *NEPS* subclades, respectively, were parsed from a corresponding multiple sequence alignment (methods above) and manually edited as necessary to remove gaps in the subsampled alignment. A new ML tree was inferred from each alignment with RAxML version 8.2.10 (68) and the GTRGAMMA model. The resulting *PRISE* and *NEPS* trees were rooted with sequences from *Petrea volubilis* L. (PEVO_c39703_g1_i1) and *Lancea tibetica* Hook.f. & Thomson (LATI_c23199_g1_i1) + *Aureolaria pectinata* (Nutt.) Pennell (AUPE_c43669_g1_i1), respectively, and used for divergence time estimation. All dating analyses used a relaxed clock approach, as implemented in treePL (69) with PL (70). Optimization parameters for each analysis were identified using the “prime” option in treePL, followed by a “thorough” analysis using those parameters. A smoothing parameter for each analysis was determined by cross-validation. We used the following age constraints for each estimation procedure: a minimum and maximum age of 25.31 and 25.63 Ma for the crown node of Nepetinae; a minimum age of 47.8 Ma for the crown node of Nepetoideae; a minimum and maximum age of 59.99 and 70.94 Ma, respectively, for the crown node of Lamiaceae; and a maximum age of 107 Ma for the root node, representing the Lamiales crown.

The age constraint for Nepetinae corresponded to the lower and upper bounds of the 95% confidence interval of estimated ages for the Nepetinae crown derived from a Lamiaceae divergence time analysis (methods below). The age constraint for Nepetoideae corresponded to the fossil pollen of *Ocimum* (71), whereas the remaining constraints corresponded to the lower and upper bounds of the 96% highest posterior density interval of estimated ages for the Lamiaceae crown (72) and the oldest estimated age reported for the Lamiales crown (73), respectively. We conducted additional dating analyses to provide 95% confidence intervals [e.g., see (74)] for ages estimated at internal nodes in the *PRISE* and *NEPS* trees. Model parameters and branch lengths were re-estimated with RAxML for both ML topologies using a bootstrap approach with 1000 replicates, producing a set of 1000 bootstrap phylograms with identical topologies for each dataset. We also performed a similar procedure using a species tree and corresponding data matrix for Lamiaceae

(10) to provide a secondary age calibration for the crown node of Nepetinae in the *PRISE* and *NEPS* divergence time analyses. However, given the robust support for the species tree topology and large matrix size, we used only 100 bootstrap replicates for the analysis. All bootstrap trees were dated using the approach described above (i.e., excluding use of the Nepetinae constraint in the species tree analyses), and age statistics at all internal nodes were summarized across each tree set with TreeAnnotator version 1.10.4 (<http://beast.community/treeannotator>).

SUPPLEMENTARY MATERIALS

Supplementary material for this article is available at <http://advances.sciencemag.org/cgi/content/full/6/20/eaba0721/DC1>

REFERENCES AND NOTES

1. A. O. Tucker, S. S. Tucker, Catnip and the catnip response I. *Econ. Bot.* **42**, 214–231 (1988).
2. S. Bol, J. Caspers, L. Buckingham, G. D. Anderson-Shelton, C. Ridgway, C. A. Buffington, S. Schulz, E. M. Bunnik, Responsiveness of cats (Felidae) to silver vine (*Actinidia polygama*), Tatarian honeysuckle (*Lonicera tatarica*), valerian (*Valeriana officinalis*) and catnip (*Nepeta cataria*). *BMC Vet. Res.* **13**, 70 (2017).
3. T. Eisner, Catnip: Its raison d’être. *Science* **146**, 1318–1320 (1964).
4. M. A. Birkett, A. Hassanali, S. Hoglund, J. Pettersson, J. A. Pickett, Repellent activity of catmint, *Nepeta cataria*, and iridoid nepetalactone isomers against Afro-tropical mosquitoes, ixodid ticks and red poultry mites. *Phytochemistry* **72**, 109–114 (2011).
5. K. Miettinen, L. Dong, N. Navrot, T. Schneider, V. Burlat, J. Pollier, L. Woittiez, S. van der Krol, R. Lugan, T. Ilc, R. Verpoorte, K.-M. Oksman-Caldentey, E. Martinoia, H. Bouwmeester, A. Goossens, J. Memelink, D. Werck-Reichhart, The seco-iridoid pathway from *Catharanthus roseus*. *Nat. Commun.* **5**, 3606 (2014).
6. F. Geu-Flores, N. H. Sherden, V. Courdavault, V. Burlat, W. S. Glenn, C. Wu, E. Nims, Y. Cui, S. E. O’Connor, An alternative route to cyclic terpenes by reductive cyclization in iridoid biosynthesis. *Nature* **492**, 138–142 (2012).
7. N. H. Sherden, B. Lichman, L. Caputi, D. Zhao, M. O. Kamileen, C. R. Buell, S. E. O’Connor, Identification of iridoid synthases from *Nepeta* species: Iridoid cyclization does not determine nepetalactone stereochemistry. *Phytochemistry* **145**, 48–56 (2018).
8. H. Kries, F. Kellner, M. O. Kamileen, S. E. O’Connor, Inverted stereocontrol of iridoid synthase in snapdragon. *J. Biol. Chem.* **292**, 14659–14667 (2017).
9. B. R. Lichman, M. O. Kamileen, G. R. Titchiner, G. Saalbach, C. E. M. Stevenson, D. M. Lawson, S. E. O’Connor, Uncoupled activation and cyclisation in catmint reductive terpenoid biosynthesis. *Nat. Chem. Biol.* **15**, 71–79 (2019).
10. Mint Evolutionary Genomics Consortium, Phylogenomic mining of the mints reveals multiple mechanisms contributing to the evolution of chemical diversity in Lamiaceae. *Mol. Plant* **11**, 1084–1096 (2018).
11. G. W. Stull, M. Schori, D. E. Soltis, P. S. Soltis, Character evolution and missing (morphological) data across Asteridae. *Am. J. Bot.* **105**, 470–479 (2018).
12. S. Dobler, G. Petschenka, H. Pankoke, Coping with toxic plant compounds - The insect’s perspective on iridoid glycosides and cardenolides. *Phytochemistry* **72**, 1593–1604 (2011).
13. J. L. Magnard, A. Rocca, J. C. Caissard, P. Vergne, P. Sun, R. Hecquet, A. Dubois, L. Hibrand-Saint Oyant, F. Jullien, F. Nicolè, O. Raymond, S. Huguet, R. Baltenweck, S. Meyer, P. Claudel, J. Jeauffre, M. Rohmer, F. Foucher, P. Huguene, M. Bendahmane, S. Baudino, Biosynthesis of monoterpene scent compounds in roses. *Science* **349**, 81–83 (2015).
14. J. Petersen, H. Lanig, J. Munkert, P. Bauer, F. Müller-Urli, W. Kreis, Progesterone 5 β -reductases/iridoid synthases (PRISE): Gatekeeper role of highly conserved phenylalanines in substrate preference and trapping is supported by molecular dynamics simulations. *J. Biomol. Struct. Dyn.* **34**, 1667–1680 (2016).
15. H. W. Nützmann, A. Huang, A. Osbourn, Plant metabolic clusters - From genetics to genomics. *New Phytol.* **211**, 771–789 (2016).
16. I. Liblikas, E. M. Santangelo, J. Sandell, P. Baeckström, M. Svensson, U. Jacobsson, C. R. Unelius, Simplified isolation procedure and interconversion of the diastereomers of nepetalactone and nepetalactol. *J. Nat. Prod.* **68**, 886–890 (2005).
17. I. Gabur, H. S. Chawla, R. J. Snowdon, I. A. P. Parkin, Connecting genome structural variation with complex traits in crop plants. *Theor. Appl. Genet.* **132**, 733–750 (2019).
18. S. Brown, M. Clastre, V. Courdavault, S. E. O’Connor, De novo production of the plant-derived alkaloid strictosidine in yeast. *Proc. Natl. Acad. Sci. U.S.A.* **112**, 3205–3210 (2015).
19. G. D. Moghe, R. L. Last, Something old, something new: Conserved enzymes and the evolution of novelty in plant specialized metabolism. *Plant Physiol.* **169**, 1512–1523 (2015).

20. B. Christ, C. Xu, M. Xu, F.-S. Li, N. Wada, A. J. Mitchell, X.-L. Han, M.-L. Wen, M. Fujita, J.-K. Weng, Repeated evolution of cytochrome P450-mediated spiroketal steroid biosynthesis in plants. *Nat. Commun.* **10**, 3206 (2019).
21. R. Huang, A. J. O'Donnell, J. J. Barbolino, T. J. Barkman, Convergent evolution of caffeine in plants by co-option of exapted ancestral enzymes. *Proc. Natl. Acad. Sci. U.S.A.* **113**, 10613–10618 (2016).
22. M. Kaltenbach, J. R. Burke, M. Dindo, A. Pabis, F. S. Munsberg, A. Rabin, S. C. L. Kamerlin, J. P. Noel, D. S. Tawfik, Evolution of chalcone isomerase from a noncatalytic ancestor. *Nat. Chem. Biol.* **14**, 548–555 (2018).
23. P. Bauer, J. Munkert, M. Brydziun, E. Burda, F. Müller-Urli, H. Gröger, Y. A. Muller, W. Kreis, Highly conserved progesterone 5 β -reductase genes (P5 β R) from 5 β -cardenolide-free and 5 β -cardenolide-producing angiosperms. *Phytochemistry* **71**, 1495–1505 (2010).
24. I. B. Rogozin, F. Belinky, V. Pavlenko, S. A. Shabalina, D. M. Kristensen, E. V. Koonin, Evolutionary switches between two serine codon sets are driven by selection. *Proc. Natl. Acad. Sci. U.S.A.* **113**, 13109–13113 (2016).
25. Y. Matsuba, T. T. Nguyen, K. Wiegert, V. Falara, E. Gonzales-Vigil, B. Leong, P. Schäfer, D. Kudrna, R. A. Wing, A. M. Bolger, B. Usadel, A. Tissier, A. R. Fernie, C. S. Barry, E. Pichersky, Evolution of a complex locus for terpene biosynthesis in *Solanum*. *Plant Cell* **25**, 2022–2036 (2013).
26. K. Miyamoto, M. Fujita, M. R. Shenton, S. Akashi, C. Sugawara, A. Sakai, K. Horie, M. Hasegawa, H. Kawaide, W. Mitsuhashi, H. Nojiri, H. Yamane, N. Kurata, K. Okada, T. Toyomasu, Evolutionary trajectory of phytoalexin biosynthetic gene clusters in rice. *Plant J.* **87**, 293–304 (2016).
27. A. M. Pohlit, N. P. Lopes, R. A. Gama, W. P. Tadei, V. F. Andrade-Neto, Patent literature on mosquito repellent inventions which contain plant essential oils—A review. *Planta Med.* **77**, 598–617 (2011).
28. G. Dawson, D. C. Griffiths, N. F. Janes, A. Mudd, J. A. Pickett, L. J. Wadhams, C. M. Woodcock, D. C. Griffiths, N. F. Janes, A. Mudd, J. A. Pickett, L. J. Wadhams, C. M. Woodcock, Identification of an aphid sex pheromone. *Nature* **325**, 614–616 (1987).
29. S. Koczor, F. Szentkirályi, M. A. Birkett, J. A. Pickett, E. Voigt, M. Tóth, Attraction of *Chrysoperla carnea* complex and *Chrysopa* spp. lacewings (Neuroptera: Chrysopidae) to aphid sex pheromone components and a synthetic blend of floral compounds in Hungary. *Pest Manag. Sci.* **66**, 1374–1379 (2010).
30. C. Li, X. L. Zhang, X. Y. Xue, F. F. Zhang, Q. Xu, X. M. Liang, Structural characterization of iridoid glucosides by ultra-performance liquid chromatography/electrospray ionization quadrupole time-of-flight tandem mass spectrometry. *Rapid Commun. Mass Spectrom.* **22**, 1941–1954 (2008).
31. C. Formisano, D. Rigano, F. Senatore, Chemical constituents and biological activities of *Nepeta* species. *Chem. Biodivers.* **8**, 1783–1818 (2011).
32. M. A. Saghai-Maroo, K. M. Soliman, R. A. Jorgensen, R. W. Allard, Ribosomal DNA spacer-length polymorphisms in barley: Mendelian inheritance, chromosomal location, and population-dynamics. *Proc. Natl. Acad. Sci. U.S.A.* **81**, 8014–8018 (1984).
33. D. Zhao, J. P. Hamilton, G. M. Pham, E. Crisovan, K. Wiegert-Rininger, B. Vaillancourt, D. Della Penna, C. R. Buell, De novo genome assembly of *Camptotheca acuminata*, a natural source of the anti-cancer compound camptothecin. *Gigascience* **6**, 1–7 (2017).
34. M. Martin, Cutadapt removes adapter sequences from high-throughput sequencing reads. *EMBnet J.* **17**, 10–12 (2011).
35. R. M. Leggett, B. J. Clavijo, L. Clissold, M. D. Clark, M. Caccamo, NextClip: An analysis and read preparation tool for Nextera Long Mate Pair libraries. *Bioinformatics* **30**, 566–568 (2014).
36. S. Gnerre, I. Maccallum, D. Przybylski, F. J. Ribeiro, J. N. Burton, B. J. Walker, T. Sharpe, G. Hall, T. P. Shea, S. Sykes, A. M. Berlin, D. Aird, M. Costello, R. Daza, L. Williams, R. Nicol, A. Gnirke, C. Nusbaum, E. S. Lander, D. B. Jaffe, High-quality draft assemblies of mammalian genomes from massively parallel sequence data. *Proc. Natl. Acad. Sci. U.S.A.* **108**, 1513–1518 (2011).
37. D. M. Bickhart, B. D. Rosen, S. Koren, B. L. Sayre, A. R. Hastie, S. Chan, J. Lee, E. T. Lam, I. Liachko, S. T. Sullivan, J. N. Burton, H. J. Huson, J. C. Nystrom, C. M. Kelley, J. L. Hutchison, Y. Zhou, J. Sun, A. Crisá, F. A. Ponce de León, J. C. Schwartz, J. A. Hammond, G. C. Waldbieser, S. G. Schroeder, G. E. Liu, M. J. Dunham, J. Shendure, T. S. Sonstegard, A. M. Phillippy, C. P. Van Tassel, T. P. Smith, Single-molecule sequencing and chromatin conformation capture enable de novo reference assembly of the domestic goat genome. *Nat. Genet.* **49**, 643–650 (2017).
38. A. C. English, S. Richards, Y. Han, M. Wang, V. Vee, J. Qu, X. Qin, D. M. Muzny, J. G. Reid, K. C. Worley, R. A. Gibbs, Mind the gap: Upgrading genomes with Pacific Biosciences RS long-read sequencing technology. *PLOS ONE* **7**, e47768 (2012).
39. B. J. Walker, T. Abeel, T. Shea, M. Priest, A. Abouelliel, S. Sakthikumar, C. A. Cuomo, Q. Zeng, J. Wortman, S. K. Young, A. M. Earl, Pilon: An integrated tool for comprehensive microbial variant detection and genome assembly improvement. *PLOS ONE* **9**, e112963 (2014).
40. F. A. Simão, R. M. Waterhouse, P. Ioannidis, E. V. Kriventseva, E. M. Zdobnov, BUSCO: Assessing genome assembly and annotation completeness with single-copy orthologs. *Bioinformatics* **31**, 3210–3212 (2015).
41. D. Zhao, J. P. Hamilton, W. W. Bhat, S. R. Johnson, G. T. Godden, T. J. Kinser, B. Boachon, N. Dudareva, D. E. Soltis, P. S. Soltis, B. Hamberger, C. R. Buell, A chromosomal-scale genome assembly of *Tectona grandis* reveals the importance of tandem gene duplication and enables discovery of genes in natural product biosynthetic pathways. *Gigascience* **8**, giz005 (2019).
42. M. S. Campbell, M. Law, C. Holt, J. C. Stein, G. D. Moghe, D. E. Hufnagel, J. Lei, R. Achawanantakun, D. Jiao, C. J. Lawrence, D. Ware, S. H. Shiu, K. L. Childs, Y. Sun, N. Jiang, M. Yandell, MAKER-P: A tool kit for the rapid creation, management, and quality control of plant genome annotations. *Plant Physiol.* **164**, 513–524 (2014).
43. J. Jurka, V. V. Kapitonov, A. Pavlicek, P. Klonowski, O. Kohany, J. Walichiewicz, Repbase update, a database of eukaryotic repetitive elements. *Cytogenet. Genome Res.* **110**, 462–467 (2005).
44. D. Kim, G. Pertea, C. Trapnell, H. Pimentel, R. Kelley, S. L. Salzberg, TopHat2: Accurate alignment of transcriptomes in the presence of insertions, deletions and gene fusions. *Genome Biol.* **14**, R36 (2013).
45. M. G. Grabherr, B. J. Haas, M. Yassour, J. Z. Levin, D. A. Thompson, I. Amit, X. Adiconis, L. Fan, R. Raychowdhury, Q. Zeng, Z. Chen, E. Mauceli, N. Hacohen, A. Gnirke, N. Rhind, F. di Palma, B. W. Birren, C. Nusbaum, K. Lindblad-Toh, N. Friedman, A. Regev, Full-length transcriptome assembly from RNA-Seq data without a reference genome. *Nat. Biotechnol.* **29**, 644–652 (2011).
46. M. Stanke, B. Morgenstern, AUGUSTUS: A web server for gene prediction in eukaryotes that allows user-defined constraints. *Nucleic Acids Res.* **33**, W465–W467 (2005).
47. B. J. Haas, J. R. Wortman, C. M. Ronning, L. I. Hannick, R. K. Smith Jr., R. Maiti, A. P. Chan, C. Yu, M. Farzad, D. Wu, O. White, C. D. Town, Complete reannotation of the *Arabidopsis* genome: methods, tools, protocols and the final release. *BMC Biol.* **3**, 7 (2005).
48. C. Trapnell, A. Roberts, L. Goff, G. Pertea, D. Kim, D. R. Kelley, H. Pimentel, S. L. Salzberg, J. L. Rinn, L. Pachter, Differential gene and transcript expression analysis of RNA-seq experiments with TopHat and Cufflinks. *Nat. Protoc.* **7**, 562–578 (2012).
49. S. R. Eddy, HMMER user's guide (2010); <ftp://selab.janelia.org/pub/software/hmmer3/>.
50. Y. Wang, H. Tang, J. D. DeBarry, X. Tan, J. Li, X. Wang, T. H. Lee, H. Jin, B. Marler, H. Guo, J. C. Kissinger, A. H. Paterson, MScanX: A toolkit for detection and evolutionary analysis of gene synteny and collinearity. *Nucleic Acids Res.* **40**, e49 (2012).
51. L. Meisel, B. Fonseca, S. González, R. Baeza-Yates, V. Cambiazo, R. Campos, M. González, A. Orellana, J. Retamales, H. Silva, A rapid and efficient method for purifying high quality total RNA from peaches (*Prunus persica*) for functional genomics analyses. *Biol. Res.* **38**, 83–88 (2005).
52. R Core Team, R: A language and environment for statistical computing. (2018); www.r-project.org/.
53. R. Wehrens, L. M. C. Buydens, Self- and super-organizing maps in R: The kohonen Package. *J. Stat. Softw.* **21**, (2007).
54. R. Kolde, heatmap: Pretty Heatmaps (2019).
55. T. T. Dang, J. Franke, E. Tatsis, S. E. O'Connor, Dual catalytic activity of a cytochrome p450 controls bifurcation at a metabolic branch point of alkaloid biosynthesis in *Rauwolfia serpentina*. *Angew. Chem. Int. Ed.* **56**, 9440–9444 (2017).
56. J. X. Chin, B. K. Chung, D. Lee, Codon Optimization OnLine (COOL): a web-based multi-objective optimization platform for synthetic gene design. *Bioinformatics* **30**, 2210–2212 (2014).
57. K. Katoh, D. M. Standley, MAFFT multiple sequence alignment software version 7: Improvements in performance and usability article fast track. *Mol. Biol. Evol.* **30**, 772–780 (2013).
58. L. T. Nguyen, H. A. Schmidt, A. Von Haeseler, B. Q. Minh, IQ-TREE: A fast and effective stochastic algorithm for estimating maximum-likelihood phylogenies. *Mol. Biol. Evol.* **32**, 268–274 (2015).
59. S. Kalyaanamoorthy, B. Q. Minh, T. K. F. Wong, A. von Haeseler, L. S. Jermini, ModelFinder: Fast model selection for accurate phylogenetic estimates. *Nat. Methods* **14**, 587–589 (2017).
60. D. T. Hoang, O. Chernomor, A. Von Haeseler, B. Q. Minh, L. S. Vinh, UFBoot2: Improving the ultrafast bootstrap approximation. *Mol. Biol. Evol.* **35**, 518–522 (2017).
61. M. N. Price, P. S. Dehal, A. P. Arkin, FastTree 2—Approximately maximum-likelihood trees for large alignments. *PLOS ONE* **5**, e9490 (2010).
62. I. Letunic, P. Bork, Interactive Tree Of Life (iTOL) v4: Recent updates and new developments. *Nucleic Acids Res.* **47**, W256–W259 (2019).
63. J. T. Simpson, K. Wong, S. D. Jackman, J. E. Schein, S. J. M. Jones, I. Birol, ABySS: A parallel assembler for short read sequence data. *Genome Res.* **19**, 1117–1123 (2009).
64. A. Loytynoja, N. Goldman, Phylogeny-aware gap placement prevents errors in sequence alignment and evolutionary analysis. *Science* **320**, 1632–1635 (2008).
65. H. Ashkenazy, O. Penn, A. Doron-Faigenboim, O. Cohen, G. Cannarozzi, O. Zomer, T. Pupko, FastML: A web server for probabilistic reconstruction of ancestral sequences. *Nucleic Acids Res.* **40**, W580–W584 (2012).
66. Z. Yang, PAML 4: Phylogenetic analysis by maximum likelihood. *Mol. Biol. Evol.* **24**, 1586–1591 (2007).

67. Z. Yang, R. Nielsen, Mutation-selection models of codon substitution and their use to estimate selective strengths on codon usage. *Mol. Biol. Evol.* **25**, 568–579 (2008).
68. A. Stamatakis, RAxML version 8: A tool for phylogenetic analysis and post-analysis of large phylogenies. *Bioinformatics* **30**, 1312–1313 (2014).
69. S. A. Smith, B. C. O'Meara, TreePL: Divergence time estimation using penalized likelihood for large phylogenies. *Bioinformatics* **28**, 2689–2690 (2012).
70. M. J. Sanderson, Estimating absolute rates of molecular evolution and divergence times: A penalized likelihood approach. *Mol. Biol. Evol.* **19**, 101–109 (2002).
71. R. K. Kar, On the Indian origin of *Ocimum* (Lamiaceae): A palynological approach. *Palaeobotanist* **43**, 43–50 (1996).
72. G. Yao, B. T. Drew, T. S. Yi, H. F. Yan, Y. M. Yuan, X. J. Ge, Phylogenetic relationships, character evolution and biogeographic diversification of *Pogostemon* s.l. (Lamiaceae). *Mol. Phylogenet. Evol.* **98**, 184–200 (2016).
73. S. B. Janssens, E. B. Knox, S. Huysmans, E. F. Smets, V. S. F. T. Merckx, Rapid radiation of *Impatiens* (Balsaminaceae) during Pliocene and Pleistocene: Result of a global climate change. *Mol. Phylogenet. Evol.* **52**, 806–824 (2009).
74. M. J. Sanderson, r8s: inferring absolute rates of molecular evolution and divergence times in the absence of a molecular clock. *Bioinformatics* **19**, 301–302 (1996).
75. B. Li, P. D. Cantino, R. G. Olmstead, G. L. C. Bramley, C.-L. Xiang, Z.-H. Ma, Y.-H. Tan, D.-X. Zhang, A large-scale chloroplast phylogeny of the Lamiaceae sheds new light on its subfamilial classification. *Sci. Rep.* **6**, 34343 (2016).
76. B. O. Li, R. G. Olmstead, Two new subfamilies in Lamiaceae. *Phytotaxa* **313**, 222–226 (2017).
77. K. J. Vining, S. R. Johnson, A. Ahkami, I. Lange, A. N. Parrish, S. C. Trapp, R. B. Croteau, S. C. K. Straub, I. Pandelova, B. M. Lange, Draft genome sequence of *Mentha longifolia* and development of resources for mint cultivar improvement. *Mol. Plant* **10**, 323–339 (2017).
78. H. Xu, J. Song, H. Luo, Y. Zhang, Q. Li, Y. Zhu, J. Xu, Y. Li, C. Song, B. Wang, W. Sun, G. Shen, X. Zhang, J. Qian, A. Ji, Z. Xu, X. Luo, L. He, C. Li, C. Sun, H. Yan, G. Cui, X. Li, X. Li, J. Wei, J. Liu, Y. Wang, A. Hayward, D. Nelson, Z. Ning, R. J. Peters, X. Qi, S. Chen, Analysis of the genome sequence of the medicinal plant *Salvia miltiorrhiza*. *Mol. Plant* **9**, 949–952 (2016).

Acknowledgments: We thank N. Hernandez-Lozada for comments on the manuscript. We also thank Z. Yang for advice on selection analysis. We are grateful to P. Brett and L. Hill for

metabolomics support. **Funding:** Funds for this study were provided by a grant to C.R.B., N.D., S.E.O'C., D.S., and P.S.S. from the National Science Foundation Plant Genome Research Program (IOS-1444499). C.R.B. is also supported from Hatch Funds (M1CL02431). B.R.L. is supported by a UK Research and Innovation Future Leaders Fellowship (MR/S01862X/1).

Author contributions: B.R.L., C.R.B., and S.E.O'C. conceived and designed the project, with contributions from other authors. B.R.L., M.O.K., L.K.H., and C.R.-L. performed tissue metabolite analysis. B.V. and J.C.W. grew plants and isolated and sequenced DNA and RNA. J.P.H. and D.Z. assembled and annotated genomes. L.P. characterized early iridoid enzymes. B.R.L. and M.O.K. characterized NEPS and PRISE enzymes. B.R.L. performed basic phylogenetic tree inference, selection analysis, and ASR. G.T.G., M.S., and T.J.K. performed molecular clock analysis with input from D.E.S. and P.S.S. All authors analyzed data. B.R.L., C.R.B., and S.E.O'C. wrote the manuscript, with contributions from all other authors. **Competing interests:** B.R.L. and S.E.O'C. have filed patent applications covering the use of some genes reported here (WO2019224536). The authors declare that they have no other competing interests. **Data and materials availability:** All data needed to evaluate the conclusions in the paper are present in the paper and/or the Supplementary Materials. Additional data related to this paper may be requested from the authors. Raw sequence reads are available in the National Center for Biotechnology Information under BioProject IDs PRJNA359989, PRJNA529676, PRJNA529674, and PRJNA557218. The three genome assemblies, annotated genes/transcripts/peptides/functional annotation, expression matrices, gff files, gene sequences, primer sequences, gene alignments, phylogenetic trees, FastML output, dating analysis data and LC-MS files are available at the Dryad Digital Repository (doi:10.5061/dryad.88tj450). GenBank accession numbers related to this work are MT108261 to MT108293.

Submitted 1 November 2019

Accepted 2 March 2020

Published 13 May 2020

10.1126/sciadv.aba0721

Citation: B. R. Lichman, G. T. Godden, J. P. Hamilton, L. Palmer, M. O. Kamileen, D. Zhao, B. Vaillancourt, J. C. Wood, M. Sun, T. J. Kinser, L. K. Henry, C. Rodriguez-Lopez, N. Dudareva, D. E. Soltis, P. S. Soltis, C. R. Buell, S. E. O'Connor, The evolutionary origins of the cat attractant nepetalactone in catnip. *Sci. Adv.* **6**, eaba0721 (2020).

The evolutionary origins of the cat attractant nepetalactone in catnip

Benjamin R. Lichman, Grant T. Godden, John P. Hamilton, Lira Palmer, Mohamed O. Kamileen, Dongyan Zhao, Brienne Vaillancourt, Joshua C. Wood, Miao Sun, Taliesin J. Kinser, Laura K. Henry, Carlos Rodriguez-Lopez, Natalia Dudareva, Douglas E. Soltis, Pamela S. Soltis, C. Robin Buell and Sarah E. O'Connor

Sci Adv 6 (20), eaba0721.
DOI: 10.1126/sciadv.aba0721

ARTICLE TOOLS	http://advances.sciencemag.org/content/6/20/eaba0721
SUPPLEMENTARY MATERIALS	http://advances.sciencemag.org/content/suppl/2020/05/11/6.20.eaba0721.DC1
REFERENCES	This article cites 74 articles, 13 of which you can access for free http://advances.sciencemag.org/content/6/20/eaba0721#BIBL
PERMISSIONS	http://www.sciencemag.org/help/reprints-and-permissions

Use of this article is subject to the [Terms of Service](#)

Science Advances (ISSN 2375-2548) is published by the American Association for the Advancement of Science, 1200 New York Avenue NW, Washington, DC 20005. The title *Science Advances* is a registered trademark of AAAS.

Copyright © 2020 The Authors, some rights reserved; exclusive licensee American Association for the Advancement of Science. No claim to original U.S. Government Works. Distributed under a Creative Commons Attribution NonCommercial License 4.0 (CC BY-NC).